

The circumstellar environment of T Tau S at high spatial and spectral resolution

G. Duchêne¹

Laboratoire d'Astrophysique, Observatoire de Grenoble, BP 53, F-38041 Grenoble cedex 9, France

gaspard.duchene@obs.ujf-grenoble.fr

A. M. Ghez, C. McCabe

Department of Physics and Astronomy, UCLA, Los Angeles, CA 90095-1562, USA

C. Ceccarelli

Laboratoire d'Astrophysique, Observatoire de Grenoble, BP 53, F-38041 Grenoble cedex 9, France

ABSTRACT

We have obtained the first high spatial ($0''.05$) and spectral ($R \sim 35000$) resolution $2\mu\text{m}$ spectrum of the T Tau S tight binary system using adaptive optics on the Keck II telescope. We have also obtained the first 3.8 and $4.7\mu\text{m}$ images that resolve the three components of the T Tau multiple system, as well as new 1.6 and $2.2\mu\text{m}$ images. Together with its very red near-infrared colors, the spectrum of T Tau Sb shows that this T Tauri star is extinguished by a roughly constant extinction of $A_V \sim 15$ mag, which is probably the $0''.7 \times 0''.5$ circumbinary structure recently observed in absorption in the ultraviolet. T Tau Sa, which is also observed through this screen and is actively accreting, further possesses a small edge-on disk that is evidenced by warm (390 K), narrow overtone CO rovibrational absorption features in our spectrum. We find that T Tau Sa is most likely an intermediate-mass star surrounded by a semi-transparent 2–3 AU-radius disk whose asymmetries and short Keplerian rotation explain the large photometric variability of the source on relatively short timescales. We also show that molecular hydrogen emission exclusively arises from the gas that surrounds T Tau S and that its spatial and kinematic structure, while providing suggestive evidence for a jet-like structure, is highly complex.

Subject headings: stars: individual (T Tau) — binaries: close — stars: pre-main sequence — circumstellar matter

¹Department of Physics and Astronomy, UCLA

1. Introduction

Since its discovery by Dyck, Simon & Zuckerman (1982), the companion to the prototypical low-mass young stellar object T Tau has been the subject of numerous studies and a source of many debates. In short, while T Tau S has never been detected at optical wavelengths (Gorham et al. 1992; Stapelfeldt et al. 1998a), it is much brighter in the mid-infrared than the optically bright T Tau (Ghez et al. 1991), which we will refer to as T Tau N in the following. This peculiar characteristic is typical of a handful of other objects, collectively known as infrared companions (IRC, Koresko et al. 1997). Noticeably, the bolometric luminosity of T Tau S ($12 L_\odot$, Koresko et al. 1997) is larger than that of the $2 M_\odot$ T Tau N. Furthermore, while T Tau N has remained remarkably stable in recent years after significant historical variations (Beck & Simon 2001; Beck et al. 2004), large photometric variations have been observed in T Tau S (Ghez et al. 1991; Beck et al. 2004). T Tau S has also long been known as the source of variable, polarized gyrosynchrotron radio emission (Skinner & Brown 1994).

Studying the spectral energy distribution (SED) of T Tau S, Koresko et al. (1997) found a bolometric temperature of ~ 500 K, much lower than that of a normal T Tauri star (TTS) and typical of more deeply embedded Class I protostars. However, the close vicinity and assumed coevality with T Tau N appears to rule out the possibility of T Tau S being in a much less evolved stage. Koresko et al. therefore proposed that T Tau S is a normal TTS, possibly slightly more massive than T Tau N, that is embedded within a compact opaque envelope responsible for a (variable) $A_V \sim 35$ mag. If its envelope is not larger than a few 100 AU, then one can argue that this is a different, later, evolutionary stage than Class I protostars, whose envelopes typically extend over several thousand AU (Motte, André & Neri 1998; Motte & André 2001).

Ghez et al. (1991), van den Ancker (1999) and Beck et al. (2004) have used the depth of the $10 \mu\text{m}$ silicate and $3 \mu\text{m}$ ice absorption features in the spectrum of T Tau S to estimate an extinction ranging from $A_V = 5$ to 30 mag with significant variations over time. For comparison, the extinction to T Tau N is estimated to be $A_V \sim 1.4\text{--}1.5$ mag (Kenyon & Hartman 1995; Koresko et al. 1997). Such large extinctions to T Tau S explain its non-detection in the optical. Beck et al. (2004) argued that the photometric variability of T Tau S can be explained by large extinction changes in our line of sight. Hogerheijde et al. (1997) have proposed that the obscuring material in front of T Tau S is the almost pole-on circumstellar disk of T Tau N. However, Akeson et al. (1998) concluded that the outer radius of T Tau N's disk is only ~ 40 AU, about half the T Tau N–T Tau S projected separation.

Another interpretation of the large variability of T Tau S is that it is in fact a FU Ori-like object in which the luminosity is entirely dominated by emission from the accretion disk (Ghez et al. 1991). Variability then arises from changes in the accretion rate on the star and the strong brightening observed in the early 1990s can be interpreted as an accretion outburst. Ghez et al.'s claim was in part based on the fact that the large flare they observed was essentially grey over the $2\text{--}10 \mu\text{m}$ range. More recently, Beck et al. (2004) found that the flux of the Br γ emission line,

which is thought to be powered by accretion, correlates with the continuum flux in a way that qualitatively agrees with this scenario. However, Beck et al. also found significant color variability for T Tau S, seemingly contradicting the FU Ori scenario.

To further complicate the picture, Koresko (2000) used speckle interferometry to identify a close ($\sim 0''.05$ or 7 AU at a 140 pc distance, Bertout et al. 1999) companion to the IRC. Such a tight separation immediately made T Tau S one of the most promising system to determine a TTS dynamical mass. Its orbital motion has been repeatedly monitored with near-infrared (Köhler et al. 2000; Duchêne, Ghez & McCabe 2002; Furlan et al. 2003; Beck et al. 2004) and radio (Loinard et al. 2003; Johnston et al. 2003, 2004) high-angular resolution techniques. Opposite claims have been made regarding the possibility that the T Tau Sa–T Tau Sb system is physically bound (Loinard et al. 2003; Furlan et al. 2003; Johnston et al. 2003, 2004; Beck et al. 2004). Although the centimeter radio observations provide a ~ 20 year time baseline, only T Tau Sb is detected at these wavelengths, requiring critical but uncertain assumptions to be made. The near-infrared datasets, on the other hand, have spatially resolved T Tau S for only the last few years. Yet, preliminary orbital solutions based exclusively on the near-infrared images, which clearly pinpoint all components of the system, suggests an orbital period on order a few decades, a periastron separation of ~ 5 –10 AU at most and a system mass of several solar masses (Beck et al. 2004). Such a large mass suggests that T Tau Sa is the most massive component of the T Tau system although it remains unclear whether its high dynamical mass can be readily reconciled with its moderate luminosity (Johnston et al. 2003). Furthermore, the fact that the most massive object has remained more deeply embedded than its lower mass close companions is also against the natural expectation of a faster clearing timescale for circumstellar material with increasing stellar mass.

From a spatially resolved moderate resolution near-infrared spectrum, T Tau Sb has been found to be a normal low-mass TTS of spectral type \sim M1 suffering from a significant extinction ($A_V \gtrsim 8$ mag, Duchêne et al. 2002). This spectrum also shows T Tau Sa to have a featureless continuum with a strong Br γ emission line synonymous of accretion. The binarity of T Tau S, combined with its strongly variable flux ratio (see Sect. 3.1; Beck et al. 2004) raises serious concern about the conclusions that can be derived from the unresolved near-infrared properties of the system. Clearly, one needs to spatially resolve the tight binary system to study the variability of both components in order to reach firm conclusions regarding their nature, since the brighter component at K has changed over time.

Some of the peculiar properties of T Tau Sa, namely its featureless K band spectrum and extremely red colors, do not apply to T Tau Sb, which appears to be a normal TTS (Duchêne et al. 2002). Therefore, the IRC phenomenon in the T Tau system is limited to T Tau Sa, and has to be contained within a volume of a few AU, even though some extinction is present in front of both components. A compact and opaque envelope could lie around that source and reprocess stellar starlight at mid-infrared wavelengths, and thereby erase any photospheric feature in its spectrum, as suggested by Koresko et al. (1997). However, the dynamical timescale for this compact envelope (free-fall time scale of a few years) to be accreted and/or dispersed is several orders of magnitude

shorter than the estimated age of the system (~ 1 Myr, White & Ghez 2001). An alternative scenario to explain the apparent faintness of T Tau Sa consists of invoking a small edge-on disk circumstellar disk. This scenario, evoked by Hogerheijde et al. (1997), Koresko (2000) and Beck et al. (2004) appeared to gain ground when Walter et al. (2003) detected an extended absorption feature that is entirely opaque to ultraviolet photons at the location of T Tau S. However, the size of this feature, ~ 70 AU, is much larger than the few AU maximal size of a circumstellar disk around T Tau Sa. Until now the location of the extinguishing material in front of T Tau Sa remains subject to debate.

Besides large quantities of dusty obscuring material, the environment of T Tau S also contains numerous evidence for mass-loss. A large and complex CO outflow is known to arise from the whole T Tau system (Edwards & Snell 1982; Schuster, Harris & Russell 1997). On smaller scales, a multi-component dynamical structure has been discovered and studied through optical emission lines by Böhm & Solf (1994) and Solf & Böhm (1999). These authors have proposed that the T Tau system is the source of two distinct stellar jets: T Tau N would drive an East-West jet that almost points to the observer whereas T Tau S would be the source for a North-South jet that extends in the plane of the sky. It is not known whether this second jet comes from T Tau Sa or T Tau Sb, though. Imaging of the near-infrared shock-excited H₂ emission line has revealed extended emission over several arcseconds (Herbst et al. 1996). On subarcsecond scales, Herbst et al. and Beck et al. (2004) detected emission arising from T Tau S but higher spatial resolution studies by Duchêne et al. (2002) and Kasper et al. (2002) found no significant emission at the stars' location. This led Beck et al. (2004) to suggest that the line emission arises only from shocked gas in the immediate surroundings of the two stars, in area small enough to be unresolved in direct imaging studies with resolution $\sim 1''$, but large enough to be resolved out in higher angular studies. Using narrow-band high angular resolution images, Quirrenbach & Zinnecker (1997) argued that some of the complex spatially resolved H₂ emission may arise from a different structure than a stellar outflow. Stapelfeldt et al. (1998a) attempted to model the scattered light images of the reflection nebula centered on T Tau, which likely traces an outflow cavity, and found an “intermediate” inclination angle, in disagreement with the inclination of either jet identified by Solf & Böhm (1999). Overall, while mass loss clearly occurs in the environment of T Tau with at least two distinct outflows, our understanding of the actual source and physical properties of both jets is still poor.

In this paper, we present the first high spectral resolution ($R \sim 35000$), high spatial resolution ($0''.05$) study of the T Tau S tight binary system. With this dataset, we have 1) detected accretion-induced Brγ emission from both T Tau Sa and T Tau Sb, 2) shown that the H₂ emission is exclusively associated to the surrounding gas and has a highly complex kinematic and spatial structure, 3) detected ¹²CO absorption features from warm gas in the line of sight of T Tau Sa, and 4) measured radial velocities for both components of the system. We also obtained new high angular resolution 1.6 and 2.2 μm images of the system, as well as the first 3.8 and 4.7 μm images that spatially resolve all three components of T Tau. Combining the ¹²CO absorption lines with a new multicolor photometric analysis of T Tau Sb, we show that T Tau Sa is an intermediate-mass star surrounded

by a small, semi transparent, edge-on disk and that a wider, possibly circumbinary, structure is located in front of both components of T Tau S.

The plan of this paper is as follows: in Sect. 2, we present the imaging and spectroscopic datasets used in this study and their reduction procedures. In Sect. 3 and 4, we present our photometric and spectroscopic results, respectively. We discuss them in Sect. 5 and summarize our findings in Sect. 6.

2. Observations

All observations used in this study have been obtained using the adaptive optics (AO) system on the 10 m Keck II telescope (Wizinowich et al. 2000). We have obtained direct images from $1.6\,\mu\text{m}$ to $4.7\,\mu\text{m}$ that clearly resolved the three components of the system (Sect. 2.1), as well as spatially resolved high spectral resolution spectra at $2\,\mu\text{m}$ of T Tau Sa and T Tau Sb (Sect. 2.2). Here we present the instrumental setups used for these observations as well as the data reduction processes. In all observations, the optically bright T Tau N ($R = 9.2$) was used as a natural guide star for the AO system.

2.1. Near-Infrared Imaging

On 2002 December 13, we used the facility AO-dedicated near-infrared camera NIRC2 (Matthews et al. 2005, in prep.), a 1024×1024 detector for which we used the $0''.00995 \pm 0''.00005$ pixel scale (Ghez et al. 2004) and whose absolute orientation on the sky is $0^\circ.7 \pm 0^\circ.2$ (Beck et al. 2004). To avoid saturation of the stars in the $2\,\mu\text{m}$ band, we used two narrow band ($\sim 1.5\%$ bandpass) filters centered at $2.18\,\mu\text{m}$ ($\text{Br}\gamma$) and $2.28\,\mu\text{m}$ (K_{cont}), respectively. We further obtained for the first time broadband AO images of the system at $3.8\,\mu\text{m}$ (L') and $4.7\,\mu\text{m}$ (M_s). For all observations, we used the “inscribed circle” pupil mask that decreases the amount of background emission at the cost of a slight loss of resolution (the equivalent telescope diameter is 9 m). In each filter, we used a similar sequence in which the system was placed in 2 or 4 different locations on the chip and 100 short integrations (0.02–0.05 s) where coadded at each location. Shorter integrations, obtained by reading only a fraction of the array (256×264 at L' and 128×152 at M_s), were used at longer wavelengths to prevent saturation in the background.

On 2003 December 12, we obtained additional images of the system using the near-infrared imager and spectrograph NIRSPEC (McLean et al. 2000). Its 256×256 imaging detector provides a pixel scale of $0''.0168 \pm 0''.0001$ and its absolute orientation on the sky is $1^\circ.1 \pm 0^\circ.8$, as estimated by us from images of several well-studied calibration binaries. We used the K band ($2.2\,\mu\text{m}$) filter as well as an instrument-specific $1.6\,\mu\text{m}$ filter that is very similar to the standard H band filter. The same observing technique was used as during the NIRC2 observations described above.

All datasets were sky subtracted, flat-fielded, corrected for bad pixel and shift-and-added using standard IRAF² routines. The final images are presented in Figure 1. The spatial resolution, as measured from the FWHM of T Tau N in all images, is 0''.055, 0''.072, 0''.087 and 0''.107 at 2.2, 1.6, 3.8 and 4.7 μ m, respectively. All three components are clearly detected in all images, except for the *H* band image in which T Tau Sa is not detected. The two components of the \sim 0''.1 T Tau S binary are only barely resolved at *M'*. Nonetheless, it is still possible to accurately extract the astrometric and photometric properties of the binary.

For all images, we performed point spread function (PSF) fitting using T Tau N as a perfect nearby and simultaneous PSF. Uncertainties on the stars' locations and fluxes were determined from the standard deviation of the quantities obtained in each individual image. All simultaneous images yielded fully consistent astrometric measurements for both the T Tau N–T Tau Sa and T Tau Sa–T Tau Sb pairs. The astrometric uncertainties for the former, wider, pair are dominated by the detectors' calibration uncertainties whereas centroiding uncertainties lead to the dominant source of error regarding the former, tighter, binary. The astrometric results are summarized in Table 1 and the photometric results are given in Table 2. The average astrometric measurements from all filters are indicated for each run.

2.2. High-Spectral Resolution Spectroscopy

2.2.1. Instrumental setups and datasets

On 2003 December 12, we used NIRSPEC to obtain 2 μ m cross-dispersed high resolution spectra of the T Tau S binary system. As illustrated in Figure 2, we aligned the 0''.027 \times 2''.26 slit along the binary system so as to spatially disentangle the spectra of the two components. In order to obtain an absolute calibration of the radial velocities, we also observed HD 35410, an IAU radial velocity standard (spectral type G9III, $v_{rad} = 20.3$ km s⁻¹, Fehrenbach & Duflot 1980). Observations of the early A-type stars HR 1389 and HD 36150 were made with the same set-up immediately before or after T Tau S and radial velocity standard in order to measure the telluric transmission function. Each star was located at 2 to 6 different locations behind the slit to correct for bad pixels and increase the signal-to-noise ratio without saturating the stars. We obtained total integration times of 30 min for T Tau S and ranging from 40 to 120 s for HR 1389, HD 35410 and HD 36150.

We selected a single cross-disperser set-up that allowed us to place simultaneously 7 consecutive, though non-adjacent, *K* band orders on the 1024 \times 1024 spectroscopic detector for all objects. Of these, the first two correspond to the short-wavelength end of the *K* band, where strong telluric absorption features are located. The non-simultaneousness of the observations of the targets and

²IRAF is distributed by the National Optical Astronomy Observatories, which is operated by the Associations of Universities for Research in Astronomy, Inc., under contract to the National Science Foundation.

their calibration A-type star resulted in poor telluric corrections in these two orders and they are not discussed further. The wavelength range of the remaining five orders are indicated in Table 3. Our spectral coverage includes molecular (2.1218 and 2.2477 μm) and atomic (2.1661 μm) hydrogen lines, as well as three of the four $\Delta v = 2$ rovibrational ^{12}CO bandheads (2.293, 2.322 and 2.383 μm), as well as a slew of associated individual ^{12}CO transitions.

In addition to obtaining standard calibration datasets (halogen flat field lamp and adjacent sky spectrum), we obtained spectra of arc lamps that were used to determine the wavelength solution for our dataset (see Sect 2.2.3). From the measured width of unresolved arc lines, we estimate that the spectral resolution is on order $R \sim 35000$ (8.5 km s^{-1}), nominal for the 2-pixel wide slit used in our set-up. We also obtained spectra of the Fabry-Perrot “etalon” lamp which produces a spectrum with ~ 15 emission lines equally spaced in frequency in each order.

2.2.2. Data Reduction and Spectra Extraction

All steps in the data reduction were performed with IRAF tasks. The raw spectra were first sky-subtracted using a sky spectrum or, if it yielded too large or too small a residual background level, another spectrum of the same object with the star(s) at a different location. A constant value per detector quadrant was then removed to correct for small bias differences in the four amplifiers. The spectra were flat-fielded using the normalized difference between the “on” and “off” halogen lamp spectra and finally corrected for bad pixels and cosmic rays. Once these cosmetic corrections were performed, we separated each order in the spectrum using windows that encompass each of them with all of their corresponding sky area. We then corrected each order for distortion using the spectra of bright stars and of the etalon lamp lines to track the curvature of the spatial and spectral axes, respectively. After the distortion correction, the 2-dimension spectra have the spatial axis vertical and the spectral axis horizontal.

The spectra of single stars, such as the radial velocity standard or the A-type stars used for atmospheric corrections, were extracted using a $\sim 0''.4$ aperture centered on the star. For T Tau S, this was not practical as the spectra of the primary overlaps significantly on the position of the secondary and vice-versa. Both stars must be carefully deblended to obtain uncontaminated spectra. We used a custom-made routine that, for each pixel along the spectral axis of each order, fits two Gaussian profiles of equal width along the spatial axis. Because the core of the AO-produced PSF is not a perfect Gaussian, this fit is not perfect and some contamination of one component by the other is unavoidable. We find that, depending on wavelength and AO correction, the spectrum of the fainter component (T Tau Sa) can be under- or over-estimated by up to 10 % although in most cases this effect does not exceed a few percent. Lorentzian profiles were also tested but they result in noisier and more contaminated spectra.

To correct the extracted 1-dimensional spectra for telluric absorption, we used the spectra of the A-type stars, which intrinsically contain essentially no photospheric line, except for the HI Br γ

line (in order #2) which is spectrally resolved over $\gtrsim 100$ pixels given the typical rotational velocities of such objects (~ 200 km s $^{-1}$). The many narrow features observed in the spectra of the A-type stars are therefore unresolved telluric absorption features. We fitted a 20–30th order polynomial function to the continuum (and hydrogen line) across each order and divided the observed spectrum by this “continuum”. This yielded the telluric transmission function, which we normalized at unity between absorption lines. The spectra of T Tau S and HD 35410 were then divided, order by order, by their corresponding telluric transmission function to yield the final spectra used in our analysis.

The final spectra have signal-to-noise ratios on order 60–90 for T Tau Sa and 90–120 for both T Tau Sb and HD 35410, as estimated from the standard deviation of the counts within several featureless continuum windows.

2.2.3. Wavelength Calibration

Too few afterglow OH lines were present even in our 300 s individual exposures to derive an accurate wavelength solution. We therefore relied on the identification of a few (between 2 and 7) known arc lines in each order. We used each independent pair of lines to estimate the pixel size (in km s $^{-1}$) in separate sections of all orders. We found no significant systematic variations at the $\sim 3\%$ level within or between the orders. The average spectral pixel size for each order are listed in Table 3; the average and standard deviation over all orders is $\langle \delta v \rangle = 4.31 \pm 0.11$ km s $^{-1}$ /pixel.

For each order, the wavelength solution was calculated as $\lambda_n = \lambda_i \times (1 + n \delta v/c)$ where n is the running pixel number starting at 0. The values of λ_i listed in Table 3 are the average values over all identified lines in each order. Since orders #3 and #5 contains the largest number of identified arc lines (4 and 7, respectively), we used the dispersion of λ_i to estimate that the accuracy of our absolute wavelength calibration is on order 15 km s $^{-1}$; this is dominated by uncertainties on the exact rest wavelength of the arc lamp lines and on the approximative nature of the adopted wavelength solution. For all other orders, we assume that the uncertainty is the same. The frequency difference between any two consecutive etalon lamp lines was found to be constant throughout the orders at the 2.5 % level, confirming the validity of our wavelength solution.

Given the uncertainty in our absolute wavelength calibration, it is not possible to determine radial velocities directly from the measured wavelength of spectral features. Rather, we used cross-correlation with the spectrum of HD 35410, which takes full advantage of the many photospheric features located in the K band. Using entire orders in the cross-correlations yields relative pixel shifts that are accurate to within 0.2 pixel ($\lesssim 1.0$ km s $^{-1}$, see Sect. 4.5). We then transformed the pixel shifts into velocity shifts using the spectral pixel size defined above and, correcting for the Earth motion using the IRAF task *rvcorr* (the correction is on order 6.5 km s $^{-1}$), we derived the heliocentric radial velocity of each source. Since the radial velocity of HD 35410 is known to within 0.7 km s $^{-1}$ (Fehrenbach & Duflot 1980), the cross-correlation technique therefore provides an accurate estimate of the radial velocity of the components of T Tau S.

3. Imaging Results

3.1. Photometric Variability

T Tau N has not shown signs of near-infrared variability over the last decade (Beck et al. 2004), and we assumed that it was at its stable level in all bands at the time of our observations³. We therefore adopt the following photometry for T Tau N: $M_s = 2.95$, $L'_{TTN} = 4.32$, $K_{TTN} = 5.52$ and $H_{TTN} = 6.32$ (Ghez et al. 1991; Beck et al. 2004). With this simultaneous photometric reference, we can study the variability of both T Tau Sa and T Tau Sb.

The images presented in Figure 1 show that, at the time of both our observations, T Tau Sa was the faintest component of the T Tau triple system at 1.6 and 2.2 μ m, in contrast to all spatially resolved measurements of the system prior to 2002 (Koresko 2000; Duchêne et al. 2002). As shown in Figure 3, T Tau Sa is now ~ 3 mag fainter ($K \sim 9.8$) and much redder ($H - K > 4.9$) than it was at the time of the first images that spatially resolved the triple system ($K \sim 6.9$ and $H - K \sim 2.6$ in November 2000, Duchêne et al. 2002). In late 2002, T Tau Sa brightened by 1.7 magnitude at K band over only 2 months, indicating large variability on short timescale. At longer wavelengths, we also find T Tau Sa to be fainter than T Tau N, and the entire T Tau S binary system has reached its lowest L' flux since Dyck et al. (1982)'s discovery observations ($L'_{TTS} = 5.15$; see Beck et al. 2004). At M_s , the combined T Tau S system was 0.4 mag fainter than T Tau N, while all historical measurements found T Tau S to clearly dominate the flux from the system at 4.7 μ m (Ghez et al. 1991; Herbst et al. 1997). The possible physical cause(s) of this variability will be discussed in Sect. 5.

While T Tau Sa is undergoing a rapid dimming trend since late 2000 (Beck et al. 2004), T Tau Sb has varied in a much more moderate way (see Figure 3). Its K band brightness has increased from $K = 9.4$ (Koresko 2000) to $K = 8.8$ (Duchêne et al. 2002) between 1997 and 2000 and, since then, it has stabilized around $K = 8.4 \pm 0.1$. Between November 2000 and December 2003, it has also somewhat brightened in H band, from $H = 10.7$ to $H = 10.3$, so that its $H - K$ color index has only changed by 0.2 mag.

From this comparison, it is clear that the photometric behavior of both components of T Tau S is dramatically different and cannot be explained with the same model. Furthermore, since most historic photometric measurements of the unresolved T Tau S system have yielded $K < 8$, it is likely that T Tau Sa dominated most of these measurements and that the strong historic variability of the system is primarily related to T Tau Sa, a conclusion also supported by the astrometric motion of T Tau S (Beck et al. 2004).

³The same magnitude was assumed for both the K_{cont} and $Br\gamma$ narrow band filters as for the broad band K filter.

3.2. Extinction Estimates For T Tau Sb

From a lower spectral resolution $2\mu\text{m}$ spectrum taken in November 2000, we had placed a lower limit of $A_V = 8$ mag to the extinction toward our line of sight to T Tau Sb, conservatively assuming that the excess was negligible in the H band (Duchêne et al. 2002). Since Muzerolle et al. (2003) have shown that the spectrum of the $1.5\text{--}4\mu\text{m}$ excess in normal TTS is well approximated by that of a $\sim 1400\text{ K}$ blackbody, we can now obtain an accurate estimate of the actual extinction to this source for this former epoch as well as for the more recent observations presented here.

The method consists in using simultaneous photometry of T Tau Sb in two near-infrared bands (H and K or K and L' here), estimating the continuum excess contribution (“veiling”) at one of these wavelengths from a spectrum, and separating the stellar and excess brightnesses using their known spectral dependence. Given its spectral type, T Tau Sb’s photosphere is characterized by $T_{\text{eff}} = 3800\text{ K}$, and so the relative contribution of the veiling over the photosphere increases with wavelength, according to their respective Planck functions. To illustrate the method, we first revisit our extinction estimate for the Nov 2000 dataset. The observed K band veiling at that time, $r_K \sim 2$, implied an H band excess on order $r_H \sim 0.7$. In turn, this means that, while the observed color index was $H - K = 1.93$, the excess-free color index was $H - K = 1.13$. With an expected photospheric color of $(H - K)_0 = 0.18$ (e.g., Kenyon & Hartmann 1995), this implies that $A_V = 15 \pm 3$ mag assuming the Rieke & Lebofsky (1985) extinction law. The uncertainty was estimated through the quadratic sum of typical uncertainties for each parameters used in this calculation: $\sigma_{r_K} \sim 0.5$, $\sigma_{T_{\text{excess}}} \sim 100\text{ K}$, $\sigma_{T_{\text{star}}} \sim 100\text{ K}$, $\sigma(H - K)_{\text{obs}} \sim 0.1$, $\sigma(H - K)_0 \sim 0.02$ and $\sigma((A_H - A_K)/A_V) \sim 0.005$.

Our Dec 2003 spectrum of T Tau Sb shows that the $2\mu\text{m}$ excess was also about $r_K \sim 2$ (see Sect. 4.3). Using the same method as above, we derive $A_V = 12 \pm 3$ mag for this newer epoch at which we obtained both H and K band fluxes for T Tau Sb. In our Dec 2002 dataset, we can use the simultaneous K and L' band photometry of T Tau Sb, although the L' band might be contaminated by the ice absorption feature observed in the line of sight of the unresolved T Tau S system (Beck et al. 2004). Keeping this caveat in mind and assuming that the K band veiling for T Tau Sb was equal to those measured in 2000 and 2003, we derive $A_V = 17 \pm 4$ mag.

The variations in extinction during these three epochs are not significant, which is consistent with the moderate ($\lesssim 0.5$ mag) variations of T Tau Sb in both H and K bands. While this method is not accurate enough to monitor the extinction toward T Tau Sb, it confirms that this component suffered only moderate changes in extinction around an average value of $A_V \sim 15$ mag while the brightness of T Tau Sa in the H and K band dropped by > 5 mag and about 3 mag, respectively, over the 2000–2003 period.

3.3. Orbital Motion

Our December 2002 astrometric measurements presented here are fully consistent with the October and December 2002 observations of Beck et al. (2004). We find significant orbital motion within the T Tau S binary system over the year separating our two datasets. Our most recent, December 2003, astrometric measurement compares reasonably well with the preliminary orbital solutions presented by Beck et al. (their Figure 13), although it seems that T Tau Sb is curving slightly more outwards than their “possible orbital models”. This is still within the uncertainties of the orbital solution and does not prompt us to revisit their results. Overall, as Beck et al. (2004) pointed out, it is not possible yet to derive a full orbital solution only on the basis of the handful of spatially resolved near-infrared datasets, essentially because of the limited time coverage they offer. These authors showed that only a strict lower limit of $1.6 M_{\odot}$ lower limit to the total mass of the T Tau S system can be estimated for now.

The new astrometric measurements presented here have been taken about six months before and after the latest published radio astrometric measurement (Johnston et al. 2004). Our dataset can therefore help better understanding the relationship between the radio source T Tau S and both infrared components of the tight binary system. In particular, comparing the two approaches is critical as only one radio source appears to be associated to T Tau S. It has been suggested by Johnston et al. (2004) that this source, although physically associated to T Tau Sb may be displaced from it by 10–30 mas. At the time of the most recent radio observations (2003 June 23), the separation between the T Tau N and T Tau S radio sources was $0''.684 \pm 00''.006$ at position angle $193^{\circ}2 \pm 0^{\circ}6$ (Johnston et al. 2004). The average of the separations we measured in December 2002 and December 2003 between T Tau N and T Tau Sb is $0''.678 \pm 0''.005$ at position angle $191^{\circ}8 \pm 0^{\circ}7$. These two separations are only different by about 1.5σ and it is therefore not possible to conclude about a possible systematic difference between the radio and infrared sources.

4. Spectroscopic Results

In this section, we discuss the high resolution spectra obtained for the T Tau S binary system. In studying the spatially resolved spectra of T Tau Sa and T Tau Sb, we focus on the molecular (Sect. 4.1) and atomic hydrogen (Sect. 4.2) emission lines, the photospheric features (Sect. 4.3) and the gas-phase CO absorption line series (Sect. 4.4). We also determine radial velocities for both components of the system (Sect. 4.5).

4.1. Molecular Hydrogen Emission

Besides the spectra of both components, the 2-dimensional spectrum corresponding to order #1 reveals spatially extended emission in the $2.1218 \mu\text{m}$ $v = 1-0 S(1)$ H_2 line, as illustrated in

Figure 4. This emission line, resolved on larger spatial scales for this system by Herbst et al. 1996), is usually detected in jets emanating from TTS and more embedded young stellar objects and studying its spatial and velocity structure can provide high spatial resolution information on the outflows in the vicinity of T Tau S.

The spectra of both components show weak H₂ emission lines, with equivalent widths (EWs) on order 0.4 and 0.15 Å for T Tau Sa and T Tau Sb, respectively. The intensity of these lines, however, is not larger than the emission from the gas in the vicinity of the stars and it is possible that no significant emission is associated to the point sources. To better isolate the line emission, we fitted and subtracted a 2nd-order polynomial function representing the spectral continuum at each pixel along the spatial direction. The result of this subtraction is presented in the right panel of Figure 4, where only the line emission and small residuals at the position of T Tau Sb (which has a spectrum that contains photospheric features which are not fitted here) are detected. There is no detectable emission left at the location of either component, providing a clear confirmation of the idea put forth by Beck et al. (2004) that the line emission seen in lower spatial resolution spectra was mistakenly attributed to the stars. Rather, it is clear from our data that all the emission can be attributed to excited gas in the vicinity of the binary system: this emission can be traced at least over 1'' on each side of the binary and the brightest emission peak is offset by $\sim 0''.4$ from T Tau Sb.

The kinematics of the gas surrounding the two stars can be analyzed from the 2-dimensional spectrum (position-velocity diagram) shown in Figure 4. We have extracted the emission spectrum in contiguous windows on both sides of the binary system; these spectra are presented in Figure 5. In these spectra, we have used the heliocentric radial velocity of T Tau Sb ($+21.1 \text{ km s}^{-1}$, see Sect. 4.5) as zero velocity reference. The velocity structure of the H₂ emission around T Tau S proves remarkably complex. On the western side of the system, the line emission is seen to gradually blueshift at increasing distance from the stars, by about 10 km s^{-1} over $\sim 0''.5$, before returning to the velocity observed close to the stars. Several separate peaks of emission can be identified along this direction. On the eastern side of the binary, the line emission appears to fork into two components, one of which becoming increasing bluer by about 10 km s^{-1} over the first $0''.4$, i.e. slightly faster than on the western side, before gradually disappearing. The other component remains at a more or less constant velocity over $\gtrsim 1''$.

The $2.2477 \mu\text{m}$ $v = 2-1 S(1)$ H₂ line is included in order #3 in our dataset. However, we fail to detect it, indicating that it is at least 17 times (3σ) fainter than the $v = 1-0 S(1)$ line on either side of T Tau S. On the other hand, the $2.2233 \mu\text{m}$ $v = 1-0 S(0)$ line is located between orders #1 and 2 and cannot be studied here; we note, however, that this line was never detected in this system however (e.g., Beck et al. 2004).

The spatial extension of the $v = 1-0 S(1)$ emission line is fully consistent with the findings of Herbst et al. (1996), but we now also have access to kinematic information to study the structure of the gas around T Tau S; we discuss this in Sect. 5.2. It is not immediately clear how the H₂

emission we detect here relates to spatially resolved emission from past studies. For instance, the northern component (N1) of the fluorescent ultraviolet emission found by Saucedo et al. (2003), which they interpret as arising from shock-excited regions in the envelope of a wide-angle outflow, appears spatially coincident with the infrared emission we detect to the west of the T Tau S system. On the other hand, the detailed studies of optical forbidden line emission by Solf & Böhm (1994) and Böhm & Solf (1999) revealed that two kinematic components (B and D, respectively associated to the collimated E-W and N-S jet) could be spatially connected with our observations at the West and East end of the slit, respectively. The velocities they measure are much larger than those derived here, but this would be a natural behavior due to the lower excitation (e.g., lower velocity shocks) conditions required for the H₂ emission line (e.g., Davis et al. 2001).

4.2. Atomic Hydrogen Emission

The spectra from order #2 contains the atomic hydrogen Br γ emission line, a tracer frequently used to study accretion in young stellar objects based on its strength (Muzeolle et al. 1998) and spectral profile (Folha & Emerson 2001). As shown in Figure 6, both components show clear Br γ emission, with T Tau Sb displaying the strongest line. Despite its weakness, the emission line in the spectrum of T Tau Sa can be identified even in single cuts along the spectra at the location of that component and it cannot result from contamination by the strong emission line of T Tau Sb. As opposed to the molecular hydrogen emission line, the Br γ line is not spatially extended with respect to the nearby continuum, showing that the emitting region is much smaller than our spatial resolution of 0''.05.

The emission line properties are summarized in Table 4. The Br γ EW is 6.2 and 0.8 \AA for T Tau Sb and T Tau Sa, respectively. These values are typical of accreting TTS (Muzeolle et al. 1998). While the EW of T Tau Sb has only marginally decreased with respect to our November 2000 observations (Duchêne et al. 2002), the line strength has strongly decreased for T Tau Sa. We are not aware of other spatially resolved line strength measurements to further analyze the amplitude of its variation on either component. However, it must be emphasized that EWs is insensitive to the line-of-sight extinction and therefore the observed variations for T Tau Sa can only be explained by an intrinsic change in line strength, and therefore in accretion properties.

The line profiles are wide: their FWHM are \sim 150 km s $^{-1}$ and their 10% (“zero”) full width at zero intensity (FWZI) range from 275 to 500 km s $^{-1}$. The profiles are roughly symmetrical, although the blue side of the line has an EW 2.5–3 stronger than the red side for both components. Furthermore, both emission lines extend to significantly larger velocities in their red wing than in their blue wing. Finally, the line peak for T Tau Sb is significantly blueshifted with respect to its rest velocity. From these properties, both objects can therefore be classified as “type I” in the denomination of Folha & Emerson (2001). These authors have shown that this group is the most frequent among TTS and the observed line profiles of T Tau Sa and T Tau Sb are representative of normal TTS. There is little doubt that, despite its unusual IRC classification, T Tau Sa is accreting

in a way that is normal for a TTS. We note however that Davis et al. (2001) found similar Br γ emission line profiles for Class I protostars so that the nature of T Tau Sa cannot be firmly ascertained from its Br γ line profile.

Since the Br γ line is assumed to be produced by gaseous material accreting onto the star, it can be used to estimate its accretion. Indeed, while the EW of the Br γ line does not correlate with accretion rate, its total flux does (Muzerolle et al. 1998; Folha & Emerson 2001). This is not practical for T Tau Sa, however, as the extinction towards this component is highly uncertain (see Sect. 5.1), and we limit our analysis to T Tau Sb. Combining the K band flux with the line EW for this component, we derive an observed (i.e., not extinction-corrected) line fluxes of $9.4 \times 10^{-17} \text{ W m}^{-2}$. After correction for an extinction of $A_V = 15$ mag (see Sect. 3.1), we estimate the accretion rate on T Tau Sb to be on order $9.2 \times 10^{-8} M_\odot \text{ yr}^{-1}$ (assuming a $2 R_\odot$ radius and $0.5 M_\odot$ mass). Using the Br γ EW and K band fluxes measured in our November 2000 spectrum (Duchêne et al. 2002) and the corresponding extinction derived above, we find that the accretion rate for T Tau Sb was essentially the same at that time.

In summary, T Tau Sb definitely appears as a normal though quite extincted TTS with a roughly constant, relatively high ($\sim 10^{-7} M_\odot \text{ yr}^{-1}$), accretion rate. On the other hand, T Tau Sa appears to be accreting at a probably variable, yet undetermined, rate.

4.3. Photospheric Features

The $2\mu\text{m}$ spectral region contains several strong features that are useful for determining the spectral type of late-type stars. Of these, the $2.20\mu\text{m}$ Na doublet and $2.26\mu\text{m}$ Ca triplet are unfortunately located in the gaps between the orders of our cross-dispersed spectra and we cannot attempt to detect them. However, orders #4 and #5 contains three overtone ($\Delta v = 2$) rovibrational ^{12}CO bandheads and numerous associated individual transitions that are prominent in late-type stars.

A lower resolution K band spectrum has already revealed many photospheric features from T Tau Sb (Duchêne et al. 2002). Our new, higher resolution spectrum also reveals the ^{12}CO bandheads from this object, as well as a suite of individual transitions between them (see Figure 7). Because our radial velocity standard giant template is of too early spectral type with respect to T Tau Sb, its spectrum contains less photospheric features, which have different strengths than that of later type dwarves (Wallace & Hinkle 1996). In fact, the CO bandheads are the only significant features that are in common to both spectra. Conveniently, M0–M1 dwarves and G8–K0 giants show CO bandheads of essentially the same strength. We can therefore compare the strength of these features in T Tau Sb and HD 35410 (spectral types M0.5 and G9III, respectively) to estimate the amount of veiling in the extincted TTS. To match the shape of the bandheads in the two objects, we needed to convolve the spectrum of the slowly rotating giant by a 6 pixel FWHM Gaussian profile, suggesting a rotational velocity of $v \sin i = 14 \pm 3 \text{ km s}^{-1}$ for T Tau Sb. After this

convolution, we find the bandheads in T Tau Sb to be about three times too weak, which implies that the veiling in Dec 2003 was $r_K \sim 2$, similar to its level in Nov 2002. This could be related to the negligible changes observed for the accretion rate on this source.

Besides the molecular and atomic emission lines (Sect. 4.1 and 4.2) and gaseous CO absorption lines (Sect. 4.4), the spectrum of T Tau Sa is remarkably featureless in all orders, despite its high signal-to-noise ratio. The tentative, very weak $v = 2-0$ rovibrational ^{12}CO bandhead at $2.29\text{ }\mu\text{m}$ in the spectrum of T Tau Sa is most likely an artifact due to contamination by the spectrum of T Tau Sb. Indeed, if this feature was real, then the other bandheads should be detected at roughly similar strengths, which is not the case. We therefore conclude that no photospheric feature typical of late-type stars has been detected in the spectrum of T Tau Sa despite our use of a much higher resolution than ever before for this source.

4.4. Gas-phase CO Absorption Lines

While the spectrum of T Tau Sa in orders #4 and #5 reveals no significant ^{12}CO bandheads, it shows a series of well-defined narrow absorption lines (Figure 7). These features, which are not detected in T Tau Sb and do not line up with telluric absorption features, cannot be the result of an improper telluric correction. Therefore, they are intrinsic to T Tau Sa. Their non-detection in our previous lower resolution spectrum of this object (Duchêne et al. 2002) can be well explained by their weakness and narrowness.

Comparing the spectrum of T Tau Sa with that of HD 35410, it appears that all absorption lines detected in the former are also present in the latter. Consequently, they are ^{12}CO transitions. Indeed, we could identify all of them using the high-spectral resolution atlas of Wallace & Hinkle (1996). They correspond to the R ($\Delta J = +1$, order #4) and P ($\Delta J = -1$, order #5) $v = 2-0$ overtone rovibrational transitions of ^{12}CO with $8 < J < 21$. In normal photospheres all these lines have essentially the same strength due to saturation effects and the series extend bluewards towards the $2.293\text{ }\mu\text{m}$ bandhead. The observed strong dependence of the line strength on the J quantum number of the initial state indicates that we are detecting absorption from a gaseous component that is much cooler than any photosphere ($T \lesssim 1500\text{ K}$).

The observed properties of the absorption lines are presented in Table 5, together with upper limits for the first undetected transitions. To derive the properties (temperature, column density) of the absorbing material, we construct a rotational diagram for the ^{12}CO molecule following the method described by Evans et al. (1991); we use the spontaneous emission coefficients listed in the HITRAN database (Rothman et al. 2003). We assume that the lines are optically thin to transform the measured equivalent widths into a column density of molecules in the state defined by a given J quantum number. The resulting rotation diagram is presented in Figure 8. Satisfyingly, the column densities derived for the R and P lines of the same initial J level agree within the errorbars.

For optically thin gas at the local thermal equilibrium (LTE), the molecules should follow a

Boltzman distribution. In the semi-logarithmic rotational diagram, all transitions should therefore be fit by a straight line, the inverse slope of which is the gas temperature. As shown in Figure 8, the measurements for all ^{12}CO lines align well along a single straight line for T Tau Sa. We take this as a proof that our assumptions of the lines being optically thin and the levels LTE-populated are correct. The first assumption is satisfied for $N_{\text{CO}} \lesssim 5 \times 10^{19} \text{ cm}^{-2}$ whereas the LTE assumption implies total gas densities larger than about 10^6 cm^{-3} . Fitting straight lines through the R and P lines provides fits that are within 1.5σ of each other in both slope and intercept. We therefore proceed to fit a single straight line to all measured lines simultaneously and derive a gas temperature of $T_{\text{gas}} = 390 \pm 15 \text{ K}$.

From the intercept, we derive a ^{12}CO column density of $9.0 \pm 1.8 \times 10^{18} \text{ cm}^{-2}$, in agreement with the optically thin assumption and well above the minimum column density required for dust- and self-shielding of the CO molecules against photodissociation by ultraviolet photons ($N_{\text{CO}}^{\text{shield}} \sim 4 \times 10^{17} \text{ cm}^{-2}$, Hollenbach & Tielens 1997). Since this gas is constrained within a $\lesssim 3 \text{ AU}$ -radius disk (see Sect. 5.1), this implies a lower limit to the CO mass of $1.3 \pm 0.3 \times 10^{-9} M_{\odot}$. Likely, the gas mass is actually larger given that our absorption measurement only intercepts a fraction of the disk because of its inclination to our line of sight. Using a typical 10^{-4} fractional abundance of ^{12}CO with respect to H_2 (e.g., Frerking, Langer & Wilson 1982), this implies a total gas mass that is larger than $9.4 \pm 1.9 \times 10^{-7} M_{\odot}$; note, however, that the actual abundance of CO in this system is unknown. Furthermore, the upper limit on the disk radius results in a lower limit to the gas density on order of $2.0 \pm 0.4 \times 10^9 \text{ cm}^{-3}$, in agreement with our LTE hypothesis. Assuming an interstellar-like gas-to-dust ratio, the amount of CO gas derived here corresponds to an extinction of $A_V \sim 90 \text{ mag}$ with the caveat that the gas-to-dust ratio could be much different value from its interstellar value. As discussed in Sect. 5.1, we believe that this warm gaseous component traces a different circumstellar component than the dusty material responsible for the reddening of the T Tau S system.

The lower excitation ^{12}CO absorption lines ($J < 8$) fall in between orders #4 and #5, so we cannot study them. A much colder gaseous component could therefore be present in our line-of-sight to T Tau Sa, as observed towards many high-mass young stellar objects (e.g., Mitchell et al. 1990), without us being able to detect it. Furthermore, we cannot determine whether ice-phase ^{12}CO is also present in the environment of this source, as it would be traced by a broad feature centered around the $P1$ line (e.g., Boogert, Hogerheijde & Blake 2002), which is outside our spectral range.

Searching for some dynamical information regarding the gas, we compare the CO absorption features profile with that of the unresolved arc lamp lines in Figure 9. All detected CO features are included in the average, in which they are weighted by their respective EW so that the deeper lines dominate the averaged profile. As opposed to the $4.7 \mu\text{m}$ CO absorption lines detected towards several young stellar objects, which frequently show blue- and/or red-shifted components (Mitchell et al. 1990; Boogert et al. 2002), the ^{12}CO lines in our spectrum of T Tau Sa are entirely unresolved and therefore do not show evidence for infall or outflow. The intrinsic linewidth of the features has

to be $\Delta v < 4 \text{ km s}^{-1}$ given that the lines do not appear broader than the unresolved arc lamps lines. Furthermore, no red or blue wing is detected; the depth of any wing extending beyond 10 km s^{-1} cannot be more than $\sim 5\%$ that of the central absorption feature.

While gaseous ^{12}CO absorption features have been detected in the M -band spectrum of three embedded young stellar objects (Mitchell et al. 1990; Boogert et al. 2002; Brittain et al. 2005), they are usually seen in emission in the spectrum of optically detected TTS and Herbig AeBe stars (Carr, Mathieu & Najita 2001; Brittain et al. 2003; Rettig et al. 2004; Thi et al. 2005). The warm, close circumstellar material traced by these emission features is seen directly by the observer thanks to the low-to-moderate inclination of these objects. More embedded sources and objects observed at high inclination provide a configuration in which CO lines are found in absorption that is much more sensitive to detect the gas. To the best of our knowledge, T Tau Sa is the second young stellar object (with HL Tau, Brittain et al. 2005) in which gas absorption features are detected at $2.3 \mu\text{m}$, despite the much weaker strength of the overtone transitions with respect to the fundamental transitions at $4.7 \mu\text{m}$, and the first in which the absorbing gas is detected within a beam size of only $0''.05$, or a mere 7 AU at the distance of T Tau S.

Encouraged by our detection of gaseous CO absorption features, we investigated the possible presence of NH_3 and CH_4 absorption features. We failed to detect the rovibrational absorption lines from the ground-state of NH_3 at $2.24719 \mu\text{m}$ (order #3) and CH_4 at $2.3075 \mu\text{m}$ (order #4) down to an equivalent width of 0.02 \AA (2σ). Assuming the same gas temperature than that derived for CO, this implies upper limits on the column densities of about $5 \times 10^{17} \text{ cm}^{-2}$, equivalent to upper limits on the abundance of these two molecules of about 5×10^{-6} .

4.5. Radial Velocities

The clear detection of photospheric features in the spectrum of T Tau Sb, combined with the high spectral resolution we achieved, allows to determine the radial velocity of that component. From the cross-correlation of T Tau Sb's spectrum with that of HD 35410 (see Figure 10), we find that the observed difference in radial velocity is 7.3 km s^{-1} . Taking into account the motion of the observatory with respect to the Sun, we find that T Tau Sb has a heliocentric radial velocity of $+21.1 \pm 1.0 \pm 0.7 \text{ km s}^{-1}$. The latter uncertainty is the systematic error introduced by the uncertainty on the velocity of the radial velocity standard and the former is the uncertainty in determining the centroid of the cross-correlation peak.

We can also use the ^{12}CO absorption features observed in the spectrum of T Tau Sa to determine a radial velocity. Again, a strongly significant peak is found in the cross-correlation between T Tau Sa and HD 35410 (see Figure 10). We find a radial velocity of $+22.0 \pm 1.0 \pm 0.7 \text{ km s}^{-1}$, a velocity that is not significantly different from that of T Tau Sb. This does not necessarily represent the radial velocity of the central object; rather it traces the velocity of material that is located in front of the star. Yet, this material is likely located in a small circumstellar disk surrounding

T Tau Sa (Sect. 5.1), and this radial velocity would then apply to the central object as well.

For comparison, the radial velocity of the optically bright T Tau N has been measured to be $+19.1 \pm 1.2 \text{ km s}^{-1}$ (Hartmann et al. 1986). Therefore, both T Tau Sa and T Tau Sb are shifted by $2\text{--}3 \text{ km s}^{-1}$ with respect to T Tau N, a shift roughly twice as small as the observed motion of the T Tau S system with respect to T Tau N in the plane of the sky ($\sim 5 \text{ km s}^{-1}$, Ghez et al. 1995; Roddier et al. 2000; Beck et al. 2004). Finally, we note that the radial velocity difference between T Tau Sa and T Tau Sb is only about 1 km s^{-1} , whereas the typical orbital velocity of the system projected in the plane of the sky is much larger, above 10 km s^{-1} (Duchêne et al. 2002; Beck et al. 2004). This implies that the orbit of T Tau Sb around T Tau Sa is essentially in the plane of the sky and/or T Tau Sb is currently close to one of its two turnaround points as seen from the Sun.

5. Discussion

5.1. T Tau Sa: An Intermediate Mass Star With an Edge-On Disk?

5.1.1. Location Of the Gas Around T Tau Sa

As demonstrated in Sect. 3.1, T Tau Sb suffers a roughly constant extinction $A_V \sim 15 \text{ mag}$. Presumably, the material that is obscuring this component also lies in our line of sight to T Tau Sa, since this component is also highly reddened. We discuss this further in Sect 5.2. For now, we focus on T Tau Sa, which we have shown behaves in a much more dramatic fashion and presents peculiar properties that have lead to its IRC classification.

The most important result of our high spectral resolution study is the discovery of the presence of warm CO gas in our line of sight to T Tau Sa. Because these absorption features are not detected in front of T Tau Sb and because the derived gas temperature is as high as $\sim 390 \text{ K}$, this gas has to be located within only a few AU of the central source. It is therefore part of the circumstellar material of T Tau Sa. The fact that the CO absorption features are very narrow ($\Delta v < 4 \text{ km s}^{-1}$) implies a dynamically stable configuration, with no significant infalling or outflowing motion. A compact envelope around T Tau Sa would evolve on a short dynamical timescale and should show large positive or negative radial velocity (depending on whether it is in infall or outflow motion) since the free-fall velocity at 5 AU of a low-mass star is larger than 10 km s^{-1} . Therefore, the circumstellar material of T Tau Sa cannot be distributed in a roughly spherical geometry.

The simplest geometry to maintain the gas at a single radial velocity is an edge-on circumstellar disk, in which the gas intercepted by our line of sight is exclusively in tangential Keplerian motion; namely such material presents no radial velocity motion⁴. If the collimated jet that lies in the plane

⁴Given the inferred small size of the disk, an “infalling disk” similar to that modeled by Hogerheijde (2001) for L1489 IRS is excluded here as the infal motion would be detectable in our line profile (see Boogert et al. 2002).

of the sky indeed arises from T Tau S (Solf & Böhm 1999), the fact that T Tau Sa may be surrounded by an edge-on disk appears as no surprise. The small size of this disk is naturally explained by the disruptive tidal forces exerted by T Tau Sb through its orbital motion (e.g., Artymowicz & Lubow 1994). The actual radius of the disk is likely to be on order 2–3 AU given the binary periastron distance (Johnston et al. 2004; Beck et al. 2004). The orbital period at the outer edge of the disk is on order of a few years at most, and our line of sight intercepts a different section of the disk within just a few weeks. The variability could therefore be explained by asymmetries within the disk, with alternatively thicker and thinner parts that move in front of us and away as the disk rotates. Given its size, this clearly is a different structure than the much larger absorbing screen found by Walter et al. (2003) and that we discuss in Sect. 5.2. Note that, since both T Tau N and T Tau Sb posses their own circumstellar disks but are not in an edge-on configuration, the three disks in this system are not parallel to each other, as already found other T Tauri multiple systems (e.g., Stapelfeldt et al. 1998b).

5.1.2. *Nature of T Tau Sa*

If there is indeed a small edge-on disk around T Tau Sa, can it explain the peculiar properties of this IRC? In particular, the featureless near-infrared spectrum, the strong variability in near-infrared brightness and color on a timescale of a few weeks only, the variable Br γ EW tracing the accretion phenomenon, and the high linear polarization rate derived by Kobayashi et al. (1997) must be accounted for. If the optical depth of the disk through its midplane is large ($\tau \gtrsim 10$), then we can only receive scattered light off the outer surface of the disk, as in other T Tauri edge-on disk systems (e.g., Burrows et al. 1996). On the other hand, if the disk opacity is small, then we receive transmitted light from both the central star and the inner rim of the disk, attenuated by the disk self-absorption. The high linear polarization rate favors a pure scattering regime, but none of the known edge-on disk shows as large a photometric variability as T Tau Sa does. A finer analysis is therefore required to derive a consistent model for this source.

When T Tau Sa fades, it also becomes much redder. This behavior, also pointed out by Beck et al. (2004) for the unresolved TTauS system over a period during which the IRC probably dominated the system in the near-infrared, suggests a change in obscuration as the main cause of the source variability. The large color change experienced by T Tau Sa when its flux varies shows that scattering is not the dominant phenomenon, as the latter introduces no time-dependent color changes. We therefore suggest that the edge-on disk surrounding T Tau Sa is only slightly or moderately opaque, with a near-infrared optical depth τ_K no larger than a few when the object is brightest. This moderate opacity ensures that scattering does not dominate in the bright state while changes of opacity of a few remain reasonable: the observed 3 magnitude drop in K band brightness for T Tau Sa implies an increase in opacity by $\Delta\tau_K \sim 3$ at that wavelength. Yet, with an opacity of a few in the near-infrared, scattering may account for a non-negligible fraction of the object’s total flux, thereby leading to a linear polarization rate of a few percent, as observed by Kobayashi et al.

(1997). We note that the column density of warm CO we have derived implies $\tau_K \sim 9$ assuming interstellar gas-to-dust and $^{12}\text{CO}/\text{H}_2$ abundance ratios. While this may be slightly too large, this is nonetheless in good agreement with the idea that the disk is only moderately optically thick.

The N band variability does not follow this “redder when fainter” trend, as already suggested by the multi-wavelength amplitude of the 1990 flare: Ghez et al. (1991) found that ~ 2 mag N band variations accompanied an equal amplitude K band flare whereas $\tau_N/\tau_K \lesssim 0.5$ for interstellar matter (Rieke & Lebofsky 1985). Furthermore, comparing a recent November 1999 N band measurement (McCabe 2004; McCabe et al. 2005, in prep.) to the late 1990 measurements of Ghez et al. (1991), we find that between the two observations, T Tau S has brightened by ~ 0.3 mag in K (Beck et al. 2004) whereas it has *faded* by ~ 0.5 mag in N . In both epochs, T Tau S was near its maximum brightness and, therefore, presumably dominated by T Tau Sa. Clearly, variable obscuration cannot account alone for the variability of T Tau Sa. We propose that the near-infrared light comes from the central source and/or the innermost regions of the circumstellar disk, and is therefore partially absorbed by the outer parts of the disk whereas the $10\ \mu\text{m}$ emission comes from further out, close to the outer edge of the small disk. This way, the fluctuations of both wavelengths may not be correlated. Variability in the N band would arise from a changing amount of material located toward the observer beyond ~ 1 AU of the central star, possibly because of outer spiral structures triggered by the orbital motion of T Tau Sb, for instance.

With the proposed geometry for T Tau Sa, the light we receive is a combination of starlight and inner disk emission, both of them suffering from absorption by the disk itself. The absence of low-mass star photospheric features in the spectrum of T Tau Sa either means that the central star is intrinsically featureless, implying a spectral type between late B and mid-F or so, or that the disk emission is much larger than that of the star itself. In the latter case, the object would be a FU Ori-like object, but our spectrum does not show the rotationally broadened ^{12}CO bandheads typical of these objects (Hartmann & Kenyon 1996), making this interpretation unlikely. We therefore favor an intermediate-to-early spectral type for T Tau Sa, making it the earliest type and consequently highest mass component of the T Tau triple system.

In its historically brightest state, in late 1999, T Tau Sa was 0.5 mag fainter at K than T Tau N (Beck et al. 2004), which in fact implies that T Tau Sa was the brightest component of the system by about 1 mag once the $A_V \sim 15$ mag extinction screen in front of T Tau S is taken into account⁵. Despite its non-detection at visible wavelengths, T Tau Sa is therefore intrinsically very bright in the near-infrared, at least at times, especially when one considers that the extinction to T Tau Sa is likely to be larger than that to T Tau Sb. In fact, at the epochs when T Tau Sa was as bright as $K \lesssim 5$ (dereddened), it was the second brightest near-infrared source in the entire Taurus star-forming region after AB Aur, a $80\ L_\odot$ B9 Herbig Be star (Kenyon & Hartmann 1995). In other

⁵Rigorously, the A_V estimate and brightest K magnitude are not simultaneous. However, at the time of our first A_V estimate, in late 2000, T Tau Sa was only 0.8 mag fainter than T Tau N at K . At that time, the dereddened flux of T Tau Sa was therefore still larger than that of T Tau N by a factor of ~ 2 .

words, T Tau Sa is most likely one of the highest mass object in the Taurus star-forming region even though it is not optically detected.

From this set of converging pieces of evidence, we suggest that T Tau Sa is an intermediate mass star with a 2–3 AU-radius edge-on disk that is partially transparent in the near-infrared. A $2.5\text{--}3 M_{\odot}$ stellar mass would be consistent with an early spectral type as well as a bright intrinsic near-infrared brightness based on the observed properties of AB Aur. The current lower limit to the dynamical mass of the system (Beck et al. 2004) is also consistent with such a mass estimate for T Tau Sa. Another consistent argument is the gas temperature we derived in Sect. 4.4: the temperature resulting from direct illumination by a 9000K photosphere is on order 270 K at 3 AU. An intermediate mass star would have a luminosity of several tens of L_{\odot} , much larger than the bolometric luminosity of T Tau Sa. This apparent light deficit could be explained by a combination of two factors. First, the edge-on disk scatters a large fraction of the optical and near-infrared starlight away from our line of sight. In the case of HH 30, Wood et al. (2002) have shown that only 10 % of the intrinsic starlight reaches the observer, resulting in a largely underestimated bolometric luminosity. The disk surrounding T Tau Sa is however only partially opaque, and so the luminosity loss is probably not as dramatic. The second factor is the presence of a foreground absorbing screen which also scatters light away from the observer (cf. Sect. 5.2). Either way, the basic argument is that the extinguishing material around T Tau Sa is not spherically symmetric and therefore our bolometric luminosity estimate, largely driven by the unextincted mid-infrared photometry, is only a lower limit to the object’s actual luminosity.

5.1.3. A Plausible Physical And Chemical Model Of The Disk Around T Tau Sa

The derived temperature (~ 390 K) and density ($\sim 2 \times 10^9 \text{ cm}^{-3}$) allow to estimate the disk mass, when they are compared with predictions of the disk structure. Indeed, the derived temperature and density compare remarkably well with the disk structure predicted by the model by Dullemond & Dominik (2004). Assuming that the disk is illuminated by a $80 L_{\odot}$ central star, following the arguments presented above, a disk with a radius of 3 AU and a mass of $0.003 M_{\odot}$ would have a warm layer of CO at about the observed density and temperature (C. Dominik, private communication). The disk would be seen at an inclination angle of about 80° , i.e., almost but not exactly edge-on. The disk mass inferred from this model is much larger than the value we have derived from the CO column density because we do not intercept the disk midplane, which would be markedly cooler (around 150 K), and, hence, we do not intercept the bulk of the disk mass with our observations. However, the inferred disk mass is satisfactorily lower than the upper limit on the T Tau S disk mass derived by Akeson et al. (1998). In practice, this comparison with a theoretical structure suggests that the disk is not seen exactly edge-on but through material located at moderate elevation above the disk midplane. This makes T Tau Sa a rare and precious source where absorption studies of the molecular content can be carried out, because the disk is not exactly edge-on, which would result in all received photons being scattered rather than transmitted

through the disk. A more detailed physical model of the disk surrounding T Tau Sa is not within the scope of the present study but would greatly help refining our understanding of this object.

The upper limits on the ammonia and methane abundances ($\leq 5 \times 10^{-6}$) are relatively stringent when compared to theoretical expectations. Both ammonia and methane are believed to be formed on the grain surfaces, by active grain chemistry (Tielens & Hagen 1982), and have indeed been observed in the solid form with abundances around $10^{-6} - 10^{-5}$ (e.g. Boogert et al. 1996; Dartois et al. 1998; Alexander et al. 2003). In the region where we observed warm CO, the dust temperature is certainly large enough to make the grain mantles sublimate. Therefore, the mantle components are injected into the gas phase, and ammonia and methane are no exception. For this reason, one would expect that the same amount of ammonia and methane seen in the ices are found in the gas phase. This is the case, for example, of ammonia whose gas phase has been measured to be of order of $10^{-6} - 10^{-5}$ in the hot cores of massive protostars and in the protostellar outflows (e.g., Bachiller 1996; Krutz et al. 2000). The same applies to methane, whose gas phase abundance in the massive hot cores has been measured to be more than 10^{-6} (e.g. Boogert, Blake & Oberg 2004). So, why we do not detect ammonia and methane at a level larger than 5×10^{-6} ? There are two possibilities. It is possible that the grain mantles around T Tau Sa have a different composition than the other mentioned environments, and are less enriched of ammonia and methane. Alternatively, chemical reactions could have removed the two molecules to form more complex molecules, which is expected in some cases in the hot cores (e.g. Charnley, Tielens & Millar 1992). Both explanations are plausible, and would have, if confirmed, interesting implications. For example, the abundance of ammonia in ices traces back to the conditions where the ices formed, namely during the pre-collapse phase, unless a vigorous reprocessing occurred during the disk phase. Further, and more sensitive observations are in need to fully explore these possibilities and the linked consequences.

5.2. On The Environment Of The T Tau S Binary System

We have found T Tau Sb to be extinguished by about $A_V \sim 15$ mag at the time of our observations, a value that changed little over the last few years. This number is similar to the extinction derived from the ice absorption feature by Beck et al. (2004), suggesting that both approaches probe the same physical structure. Estimating the depth of the mid-infrared silicate absorption feature from three narrow-band photometric measurements, Ghez et al. (1991) estimated $A_V \sim 5$ mag only. More recently, Herbst, Roberto & Beckwith (1997) found the silicate feature to be almost twice as deep, bringing this extinction estimate closer to the other ones. We note, however, that the depth of the $10 \mu\text{m}$ silicate feature only poorly correlates with A_V in molecular clouds (e.g., Whittet et al. 1988). Still, a consistent picture of the system can be proposed based on the convergent estimates of the amount of extinguishing gaseous and solid materials. As readily suggested by the non-detection of either component at visible wavelengths, there seems to be an $A_V \sim 15$ mag obscuring cloud in front of the entire T Tau S system, which we believe to be the structure seen in absorption by Walter et al. (2003). This structure, whose size is about $0''.7 \times 0''.5$, is much too large to correspond

to a circumstellar disk around either star given their small separation. It is quite possible that this is a circumbinary envelope or thick disk (*à la* GG Tau, Guilloteau, Dutrey & Simon 1999) that obscure both components. If its inner radius is at least 50 AU (or $\sim 0''.35$), it is stable with respect to the orbital motion of the inner tight binary system whereas its outer radius is probably set by the motion of T Tau N, which is located far away enough to generate only little perturbation to such a structure (Walter et al. 2003). Such a large size for the obscuring screen is also consistent with the presence of ice and silicate absorption features: only that far from the central star is the material cold enough to produce significant absorption in these features. On the other hand, the warm CO absorption features we have found in the spectrum of T Tau Sa cannot be associated with this screen, since the gas temperature 50 AU from a source with a few times $10 L_\odot$ luminosity is not higher than ~ 120 K.

We have shown that the molecular hydrogen emission from T Tau S is spatially resolved over $2''$ around the system and does not arise from the stars themselves. The linear accelerations observed in the position-velocity diagram are reminiscent of propagating jets (e.g., Hirth, Mundt & Solf 1997); however, the presence of blue-shifted components *on both sides* of the system and the narrowness of the line profiles at any spatial location argues against the emission line being excited in shocked regions of a single jet. On the other hand, the spatial coincidence between ultraviolet fluorescent line emission with the infrared line emission we detect to the West of the system argues for a similar emission mechanism; however, no ultraviolet emission seems to be directly associated with the infrared emission we detect East of the tight binary system. It is not possible to conclude on the nature of the excitation mechanism on the basis of our observations only; similar observations with different slit orientations, or integral field spectroscopic observations, would be required to determine the exact nature of the H_2 emission. In any case, our observations reveal the complex kinematic and spatial structure of the gas surrounding T Tau S.

6. Conclusion

We have used the AO-fed cross-dispersed echelle spectrograph NIRSPEC on Keck II to obtain the first high spatial ($0''.05$) and spectral ($R \sim 35000$) resolution $2\mu m$ view of the mysterious tight binary system T Tau S by aligning the entry slit along the position angle of the binary. We have further obtained the first 3.8 and $4.7\mu m$ broadband images that resolve all three components of the T Tau multiple system, as well as new 1.6 and $2.2\mu m$ images.

The spectrum of T Tau Sb confirms that it is a low-mass TTS with significant excess emission from its circumstellar disk. Its very red near-infrared colors can be explained by a roughly constant extinction on order $A_V \sim 15$ mag, in agreement with previous extinction measurements based on ice and silicate features. We believe that the obscuring material is located in a $\gtrsim 50$ AU-sized circumbinary structure, whose absorption was also recently detected in the ultraviolet.

The spectrum of T Tau Sa, on the other hand, is featureless, with the notable exceptions of

i) a weak and variable Br γ emission that probably traces accretion on the central star, and ii) a series of narrow ^{12}CO rovibrational absorption lines without their corresponding bandhead. A rotational diagram shows that the CO lines correspond to a moderate column density of gas at a temperature on order 390 K. To account for this high temperature and in the absence of evidence for infall or outflow in the gas, we believe that this material is located in a small (2–3 AU in radius) edge-on disk that surround an intermediate-mass star. The large variability of T Tau Sa in both near-infrared brightness and color cannot be uniquely accounted for by changes in the amount of line of sight extinction. Rather, we propose that the disk around T Tau Sa is moderately opaque ($\tau_K \sim$ a few) and that our line of sight intercept alternatively thicker and thinner sections of the disks as its outer radius rotates around the central star in just a few years.

Finally, we have analyzed the spatial and kinematic properties of the molecular gas in the vicinity of T Tau S, as traced by molecular hydrogen emission. We find an unusual structure in that the emission appears to gradually blueshift with distance to the stars on both sides of the binary. The exact nature of the excitation mechanism remains unknown but these results confirm the highly complex structure of the gaseous material surrounding the T Tau system.

We are grateful to our referee, T. Beck, for her detailed report that helped us clarifying several aspects of this manuscript and to C. Dominik for granting us access to unpublished details of his disk models. Data presented herein were obtained at the W. M. Keck Observatory, which is operated as a scientific partnership among the California Institute of Technology, the University of California, and the National Aeronautics and Space Administration. The Observatory was made possible by the generous financial support of the W. M. Keck Foundation. This work has been supported in part by the National Science Foundation Science and Technology Center for Adaptive Optics, managed by the University of California at Santa Cruz under cooperative agreement AST 98-76783 and by the Packard Foundation. The authors wish to extend special thanks to those of Hawaiian ancestry on whose sacred mountains we are privileged to be guests. Without their generous hospitality, none of the observations presented herein would have been possible.

REFERENCES

Akeson, R. L., Koerner, D. W., & Jensen, E. L. N. 1998, *ApJ*, 505, 358

Alexander, R. D., Casali, M. M., André, P., Persi, P. & Eiroa, C. 2003, *A&A*, 401, 613

Artymowicz, P. & Lubow, S. H. 1994, *ApJ*, 421, 651

Bachiller, R. 1996, *ARA&A*, 34, 111

Beck, T. L., Schaefer, G. H., Simon, M., Prato, L., Stoesz, J. A. & Howell, R. R. 2004, *ApJ*, 614, 235

Beck, T. L. & Simon, M. 2001, *AJ*, 122, 413

Bertout, C., Robichon, N. & Arenou, F. 1999, *A&A*, 352, 574

Böhm, K.-H. & Solf, J. 1994, *ApJ*, 430, 277

Boogert, A. C. A., Blake, G. A. & Ölberg, K. 2004, *ApJ*, 615, 344

Boogert, A. C. A., Hogerheijde, M. R. & Blake, G. A. 2002a, *ApJ*, 568, 761

Boogert, A. C. A., Schutte, W. A., Tielens, A. G. G. M., Whittet, D. C. B., Helmich, F. P., Ehrenfreund, P., Wesselius, P. R., de Graauw, T. & Prusti, T. 1996, *A&A*, 315, L377

Brittain, S. D., Rettig, T. W., Simon, T., Kulesa, C., DiSaanti, M. A. & Dello Russo, N., *ApJ*, 588, 535

Brittain, S. D., Rettig, T. W., Simon, T. & Kulesa, C., *ApJ*, in press (astro-ph/0502077)

Burrows, C. J., Stapelfeldt, K. R., Watson, A. M., Krist, J. E., Ballester, G. E., Clarke, J. T., Crisp, D., Gallagher, J. S. III, Griffiths, R. E., Hester, J. J., Hoessel, J. G., Holtzman, J. A., Mould, J. R., Scowen, P. A., Trauger, J. T. & Westphal, J. A. 1996, *ApJ*, 473, 437

Carr, J. S., Mathieu, R. D. & Najita, J. R. 2001, *ApJ*, 551, 454

Charnley, S. B., Tielens, A. G. G. M. & Millar, T. J. 1992, *ApJ*, 399, L71

Dartois, E., d'Hendecourt, L., Boulanger, F., Jourdain de Muizon, M., Breitfellner, M., Puget, J.-L. & Habing, H. J. 1998, *A&A*, 331, 651

Davis, C. J., Ray, T. P., Desroches, L. & Aspin, C. 2001, *MNRAS*, 326, 524

Duchêne, G., Ghez, A. M. & McCabe, C. 2002, *ApJ*, 568, 771

Dullemond, C. P. & Dominik, C. 2004, *A&A*, 417, 159

Dyck, H. M., Simon, T., & Zuckerman, B. 1982, *ApJ*, 255, L103

Edwards, S. & Snell, R. L. 1982, *ApJ*, 261, 151

Evans, N. J. II, Lacy, J. H. & Carr, J. S. 1991, *ApJ*, 383, 674

Fehrenbach, C. & Duflot, M. 1980, *A&AS*, 39, 311

Folha, D. F. M. & Emerson, J. P. 2001, *A&A*, 365, 90

Frerking, M. A., Langer, W. D. & Wilson, R. W. 1982, *ApJ*, 262, 590

Furlan, E., Forrest, W. J., Watson, D. M., Uchida, K. I., Brandl, B. R., Keller, L. D. & Herter, T. L. 2003, *ApJ*, 596, L87

Ghez, A. M., Wright, S. A., Matthews, K., Thompson, D., Le Mignant, D., Tanner, A., Hornstein, S. D., Morris, M., Becklin, E. E. & Soifer, B. T. 2004, *ApJ*, 601, L159

Ghez, A. M., Weinberger, A. J., Neugebauer, G., Matthews, K., & McCarthy, D. W. 1995, *AJ*, 110, 753

Ghez, A. M., Neugebauer, G., Gorham, P. W., Haniff, C. A., Kulkarni, S. R., Matthews, K., Koresko, C., & Beckwith, S. 1991, *AJ*, 102, 2066

Gorham, P. W., Ghez, A. M., Hannif, C. A., Kulkarni, S. R., Matthews, K. & Neugebauer, G. 1992, *AJ*, 103, 953

Guilloteau, S., Dutrey, A. & Simon, M. 1999, *A&A*, 348, 570

Hartmann, L. & Kenyon, S. J. 1996, *ARA&A*, 34, 207

Hartmann, L., Hewett, R., Stahler, S. & Mathieu, R. D. 1986, *ApJ*, 309, 275

Herbst, T. M., Robberto, M. & Beckwith, S. V. W. 1997, *AJ*, 114, 744

Herbst, T. M., Beckwith, S. V. W., Glindemann, A., Tacconi-Garman, L. E., Kroker, H., & Krabbe, A. 1996, *AJ*, 111, 2403

Hirth, G. A., Mundt, R. & Solf, J. 1997, *A&AS*, 126, 437

Hogerheijde, M. R. 2001, *ApJ*, 553 618

Hogerheijde, M. R., van Langevelde, H. J., Mundy, L. G., Blake, G. A., & van Dishoeck, E. F. 1997, *ApJ*, 490, L99

Hollenbach, D. J. & Tielens, A. G. G. M. 1997, *ARA&A*, 35, 179

Johnston, K. J., Fey, A. L., Gaume, R. A., Claussen, M. J. & Hummel, C. A. 2004, *AJ*, 128, 822

Johnston, K. J., Gaume, R. A., Fey, A. L., de Vegt, C. & Claussen, M. J. 2003, *AJ*, 125, 858

Kasper, M. E., Feldt, M., Herbst, T. M., Hippler, S., Ott, T. & Tacconi-Garman, L. E. 2002, ApJ, 568, 267

Kenyon, S. J. & Hartmann, L. 1995, ApJS, 101, 117

Kobayashi, N., Nagata, T., Tamura, M., Takeuchi, T., Takami, H. & Sato, S. 1997, ApJ, 481, 936

Köhler, R., Kasper, M. & Herbst, T. 2000, *in* “Birth and evolution of binary stars”, poster proceedings of IAU symp. 200, eds. B. Reipurth & H. Zinnecker, 63

Koresko, C. D. 2000, ApJ, 531, L147

Koresko, C. D., Herbst, T. M., & Leinert, Ch. 1997, ApJ, 480, 741

Kurtz, S., Cesaroni, R., Churchwell, E., Hofner, P. & Walmsley, C. M. 2000, *in* “Protostars and Planets IV”, eds. Mannings, V., Boss, A. P. & Russell, S. S., Univ. of Arizona Press, 299

Loinard, L., Rodríguez, L. F. & Rodríguez, M. I. 2003, ApJ, 578, L47

McCabe, C. 2004, Ph.D. thesis, UCLA

McLean, I. S., Graham, J. R., Becklin, E. E., Figer, D. F., Larkin, J. E., Levenson, N. A., & Teplitz, H. I. 2000, Proc. SPIE, 4008, 1048

Mitchell, G. F., Maillard, J.-P., Allen, M., Berr, R. & Belcourt, K. 1990, ApJ, 363, 554

Motte, F. & André, P. 2001, A&A, 365, 440

Motte, F., André, P. & Neri, R. 1998, A&A, 336, 150

Muzerolle, J., Calvet, N., Hartmann, L. & D'Alessio, P. 2003, ApJ, 597, L149

Muzerolle, J., Hartmann, L., & Calvet, N. 1998, AJ, 116, 2965

Quirrenbach, A. & Zinnecker, H. 1997, Proc. SPIE, 3136, 249

Rettig, T. W., Haywood, J., Simon, T., Brittain, S. D. & Gibb, E. 2004, ApJ, 616, L163

Rieke, G. H. & Lebofsky, M. J. 1985, ApJ, 288, 618

Roddier, F., Roddier, C., Brandner W., Charissoux, D., Véran, J.-P., & Courbin, F. 2000, *in* “Birth and evolution of binary stars”, poster proceedings of IAU symp. 200, eds. B. Reipurth & H. Zinnecker, 60

Rothman, L. S., et al. 2003, J. Quant. Spectrosc. Radiat. Transfer, 82, 5

Saucedo, J., Calvet, N., Hartmann, L. & Raymond, J. 2003, ApJ, 591, 275

Schuster, K.-F., Harris, A. I. & Russell, A. P. G. 1997, A&A, 321, 568

Skinner, S. L. & Brown, A. 1994, AJ, 107, 1461

Solf, J. & Böhm, K.-H. 1999, ApJ, 523, 709

Stapelfeldt, K. R., Burrows, C. J., Krist, J. E., Watson, A. M., Ballester, G. E., Clarke, J. T., Crisp, D., Evans, R. W., Gallagher, J. S. III, Griffiths, R. E., Hester, J. J., Hoessel, J. G., Holtzman, J. A., Mould, J. R., Scowen, P. A., Trauger, J. T., Westphal, J. A. 1998a, ApJ, 508, 736

Stapelfeldt, K. R., Krist, J. E., Menard, F., Bouvier, J., Padgett, D. L., & Burrows, C. J. 1998b, ApJ, 502, L65

Thi, W.-F., van Dalen, B., Bik, A. & Waters, L. B. F. M. 2005, A&A, 430, L61

Tielens, A. G. G. M. & Hagen, W. 1982, A&A, 114, 245

van den Ancker, M. E., Wesselius, P. R., Tielens, A. G. G. M., van Dishoeck, E. F. & Spinoglio, L. 1999, A&A, 348, 877

Wallace, L. & Hinkle, K. 1996, ApJS, 107, 312

Walter, F. M., Herczeg, G., Brown, A., Ardila, D. R., Gahm, G. F., Johns-Krull, C. M., Lissauer, J. J., Simon, M. & Valenti, J. A. 2003, AJ, 126, 3076

White, R. J. & Ghez, A. M. 2001, ApJ, 556, 265

Whittet, D. C. B., Bode, M. F., Longmore, A. J., Adamson, A. J., McFadzean, A. D., Aitken, D. K. & Roche, P. F. 1988, MNRAS, 233, 321

Wizinowich, P. L., Acton, D. S., Lai, O., Gathright, J., Lupton, W., & Stomski, P. J. 2000, Proc. SPIE, 4007, 2

Wood, K., Wolff, M. J., Bjorkman, J. E. & Whitney, B. 2002, ApJ, 564, 887

Table 1. New astrometric measurements in the T Tau triple system

Date	T Tau N–T Tau Sa		T Tau Sa–T Tau Sb	
	Sep. (")	Pos. Ang. (°)	Sep. (")	Pos. Ang. (°)
2002 Dec 13	$0''.695 \pm 0''.007$	$183^\circ.3 \pm 0^\circ.7$	$0''.108 \pm 0''.001$	$284^\circ.9 \pm 0^\circ.9$
2003 Dec 12	$0''.698 \pm 0''.005$	$181^\circ.9 \pm 1^\circ.2$	$0''.118 \pm 0''.002$	$288^\circ.6 \pm 1^\circ.1$

Table 2. New photometric measurements in the T Tau triple system

Date	Filter	T Tau N ^a	T Tau Sa	T Tau Sb
2002 Dec 13	K_{cont}	5.52	8.77 ± 0.03	8.33 ± 0.03
	$Br\gamma$	5.52	9.10 ± 0.03	8.48 ± 0.03
	L'	4.32	5.64 ± 0.03	6.25 ± 0.03
	M_s	2.95	3.78 ± 0.03	4.59 ± 0.05
	K	5.52	9.70 ± 0.07	8.50 ± 0.06
2003 Dec 12	H	6.32	>13.6	10.22 ± 0.11

Note. — All measurements are presented as magnitudes.

^aThe photometry for T Tau N is taken from Beck et al. (2004) at K (its magnitude in the K_{cont} and $Br\gamma$ narrow band filters is assumed equal to that of the broad band filter) and L' and from Ghez et al. (1991) at H and M ; we applied the latter flux density for our M_s photometry despite the slight bandpass mismatch.

Table 3. Instrumental set-up for the spectroscopic observations

Order #	λ_i (μm)	λ_f (μm)	δv (km s^{-1} / pixel)	Note
1	2.102321	2.132959	4.22	H_2
2	2.161989	2.193496	4.28	$\text{HI Br}\gamma$
3	2.225272	2.257702	4.32	H_2, NH_3
4	2.292261	2.325667	4.35	$^{12}\text{CO}, \text{CH}_4$
5	2.363703	2.398150	4.31	^{12}CO

Note. — λ_i , λ_f and δv represent the wavelength at the first and last pixel and pixel width along the spectral direction, respectively. The average value of δv throughout the five orders is used for wavelength calibration in our study.

Table 4. Properties of the $\text{Br}\gamma$ emission lines

	T Tau Sa	T Tau Sb
EW (\AA)	0.78 ± 0.05	6.2 ± 0.3
EW_{red} (\AA)	0.22 ± 0.05	1.6 ± 0.1
EW_{blue} (\AA)	0.56 ± 0.05	4.7 ± 0.3
FWHM (km s^{-1})	164 ± 17	147 ± 9
FWZI (km s^{-1})	275 ± 45	490 ± 43
v_{peak} (km s^{-1})	-17 ± 22	-30 ± 4
v_{red} (km s^{-1})	$+91 \pm 13$	$+177 \pm 9$
v_{blue} (km s^{-1})	-185 ± 13	-315 ± 40

Note. — EW is the total EW of the emission line while EW_{red} and EW_{blue} are the EWs of the line on either side of the rest velocity of T Tau Sb; FWHM and FWZI are the full width at half maximum and at 10% (“zero”) intensity of the emission line, respectively; v_{peak} , v_{red} and v_{blue} are the measured velocities at the line peak intensity and at the extremity of the red and blue wings, respectively. All uncertainties include uncertainties in the continuum estimates and in the exact line profile in the extended wings. Uncertainties related to the absolute wavelength calibration (velocity estimates and “red” and “blue” EWs) are not included.

Table 5. ^{12}CO 2–0 rovibrational absorption line properties

J	R lines ($\Delta J = +1$)		P lines ($\Delta J = -1$)	
	λ_{obs} (μm)	EW (\AA)	λ_{obs} (μm)	EW (\AA)
8			2.36567	0.187 ± 0.020
9			2.36825	0.158 ± 0.010
10			2.37083	0.138 ± 0.010
11	2.32519	0.150 ± 0.013	2.37345	0.130 ± 0.010
12	2.32366	0.120 ± 0.010	2.37609	0.125 ± 0.007
13	2.32218	0.097 ± 0.007	2.37875	0.109 ± 0.017
14	2.32071	0.085 ± 0.010	2.38144	0.080 ± 0.014
15	2.31931	0.073 ± 0.007	2.38416	0.084 ± 0.010
16	2.31789	0.068 ± 0.012	2.38689	0.093 ± 0.014
17	2.31657	0.072 ± 0.008	2.38967	0.086 ± 0.014
18	2.31524	0.047 ± 0.007	2.39263	0.054 ± 0.010
19	2.31397	0.033 ± 0.005		< 0.050
20	2.31276	0.040 ± 0.010		
21	2.31152	0.023 ± 0.005		
22		< 0.033		

Note. — J represents the rotational quantum number of the initial state of the transition. The R lines with $J < 11$ and P lines with $J < 8$ are outside of the wavelength range covered in our dataset. R and P lines are detected in orders # 4 and 5, respectively. For the first undetected line in each series, 3σ upper limits are given. Similar (or less constraining) upper limits apply to the following undetected lines within the observed wavelength range.

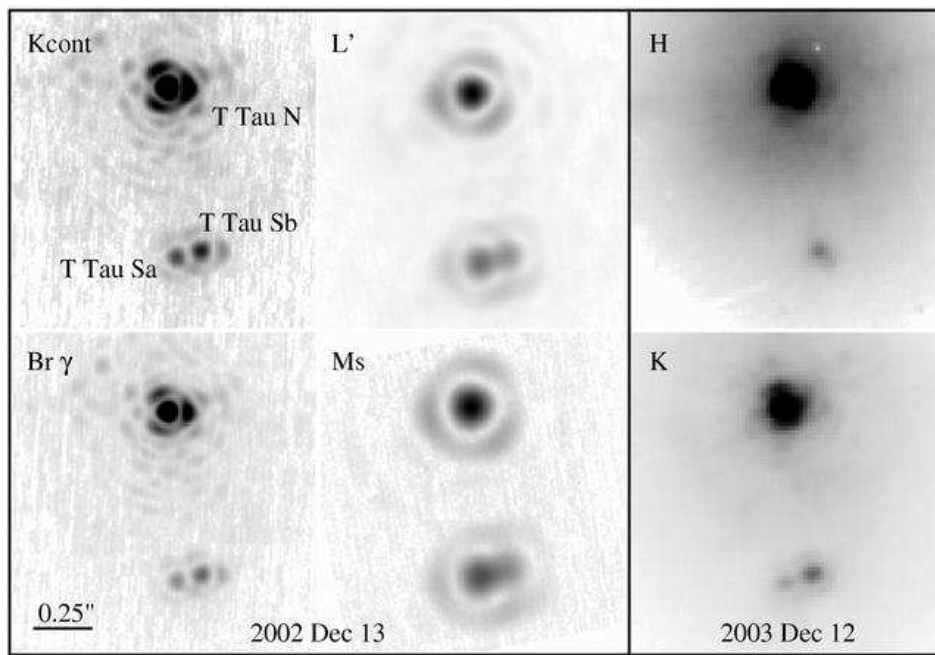


Fig. 1.— Keck adaptive optics images of T Tau, presented on a square root stretch. All images are 1''.3 on the side, oriented with North up and East to the left. Note that T Tau Sa was much redder than T Tau Sb in December 2002 and was undetected in our December 2003 *H*-band image.

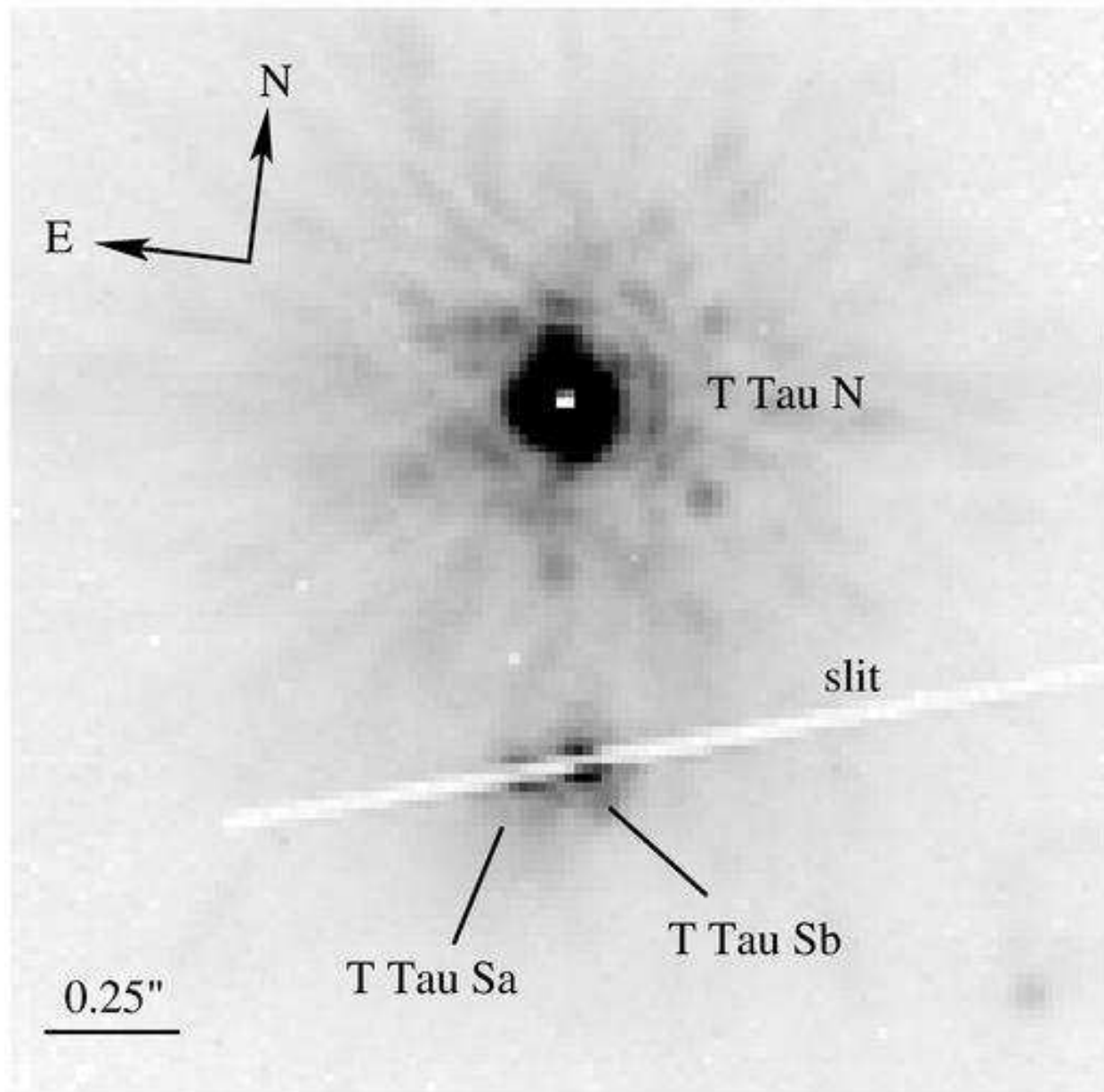


Fig. 2.— *K*-band image of the T Tau triple system obtained with the slit-viewing camera of NIRSPEC during the acquisition of the high-resolution spectra presented in this study. T Tau N is heavily saturated in this image. The image is $2''$ on the side.

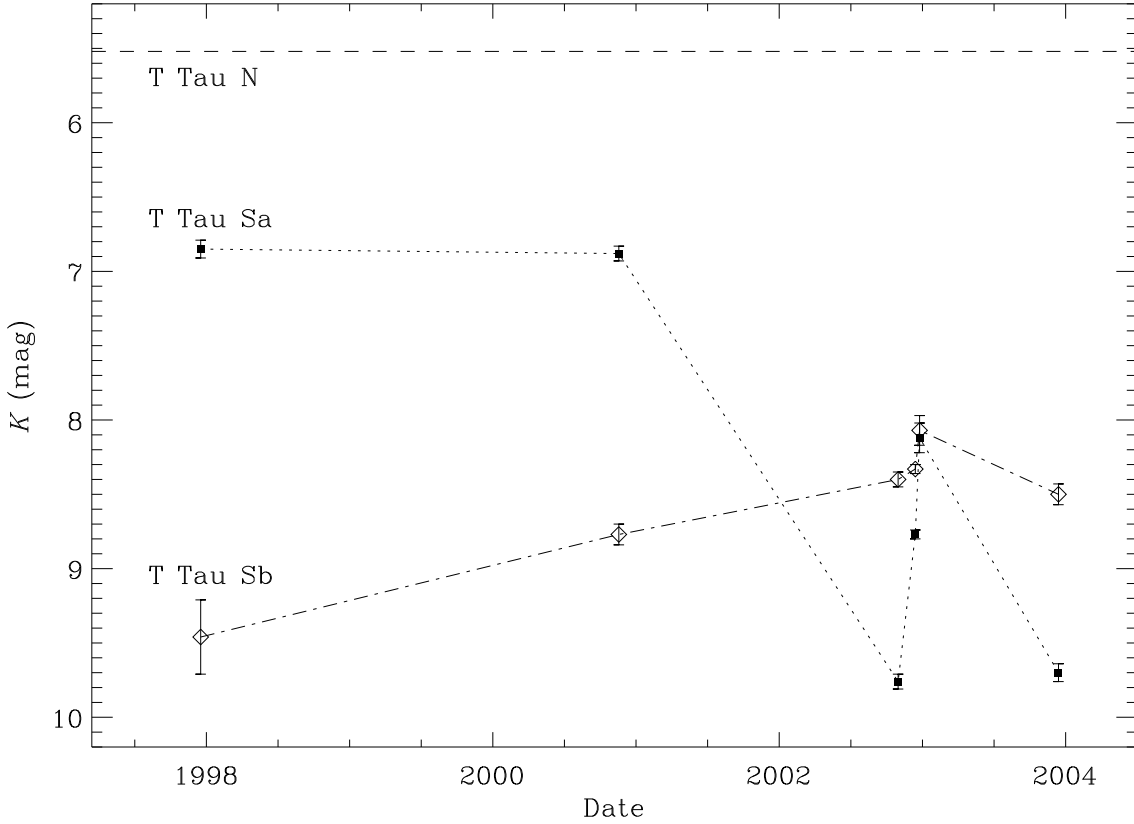


Fig. 3.— The spatially-resolved time variability of both components of T Tau S in the K band from Koresko (2000), Duchêne et al. (2002), Furlan et al. (2003), Beck et al. (2004) and this study. Filled squares and open diamonds represent T Tau Sa and T Tau Sb respectively; the dotted and dash-dotted lines should only be considered as guidelines for the eye. The dashed line represent the constant brightness of T Tau N (Beck et al. 2004). Uncertainties of 0.05 mag, 0.05 mag and 0.10 mag for the T Tau N–T Tau S flux ratios have been assumed for the Koresko (2000), Beck et al. (2004) and Furlan et al. (2003) measurements, respectively. The dramatic flux decrease of T Tau Sa between late 2000 and now has been accompanied by only minor changes in the flux of T Tau Sb.

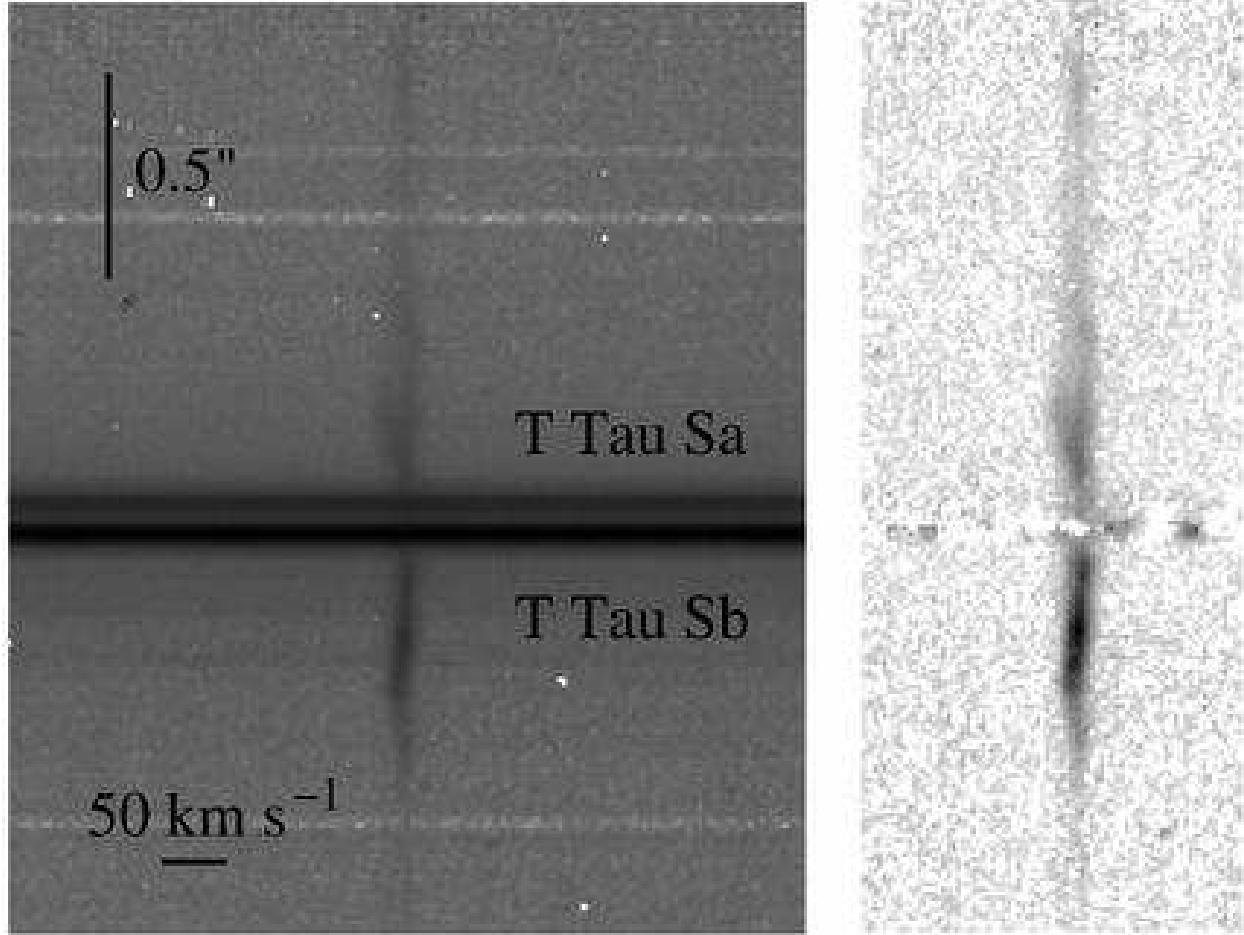


Fig. 4.— *Left:* The 2D spectrum ($3\text{''}.2$ by 700 km s^{-1}) of T Tau S around the H_2 emission line on a logarithmic stretch. The three negative stripes about $1''$ from the stars are due to faint residuals in the sky image used in the data reduction process. Note that the spectrum extends over more than one slit length because we combined images from several slit positions. *Right:* The continuum subtracted image in a 300 km s^{-1} -wide window around the H_2 emission line on a square root stretch. Note the complex velocity patterns on either side of the stars. Small residuals are left at the location of T Tau Sb because the spectrum of this object has higher frequency structure than the second-order polynomial continuum that we subtracted. No significant emission is detected at the location of either component.

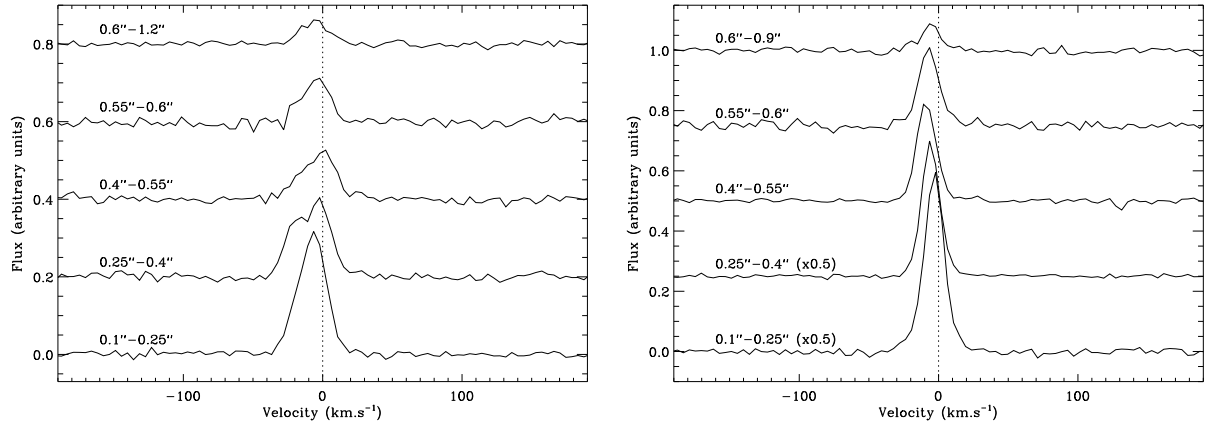


Fig. 5.— Spectra of the H₂ emission line in successive windows located on the East (*left*) and West (*right*) side of the binary system. The rest velocity of T Tau Sb is indicated by the dotted line.

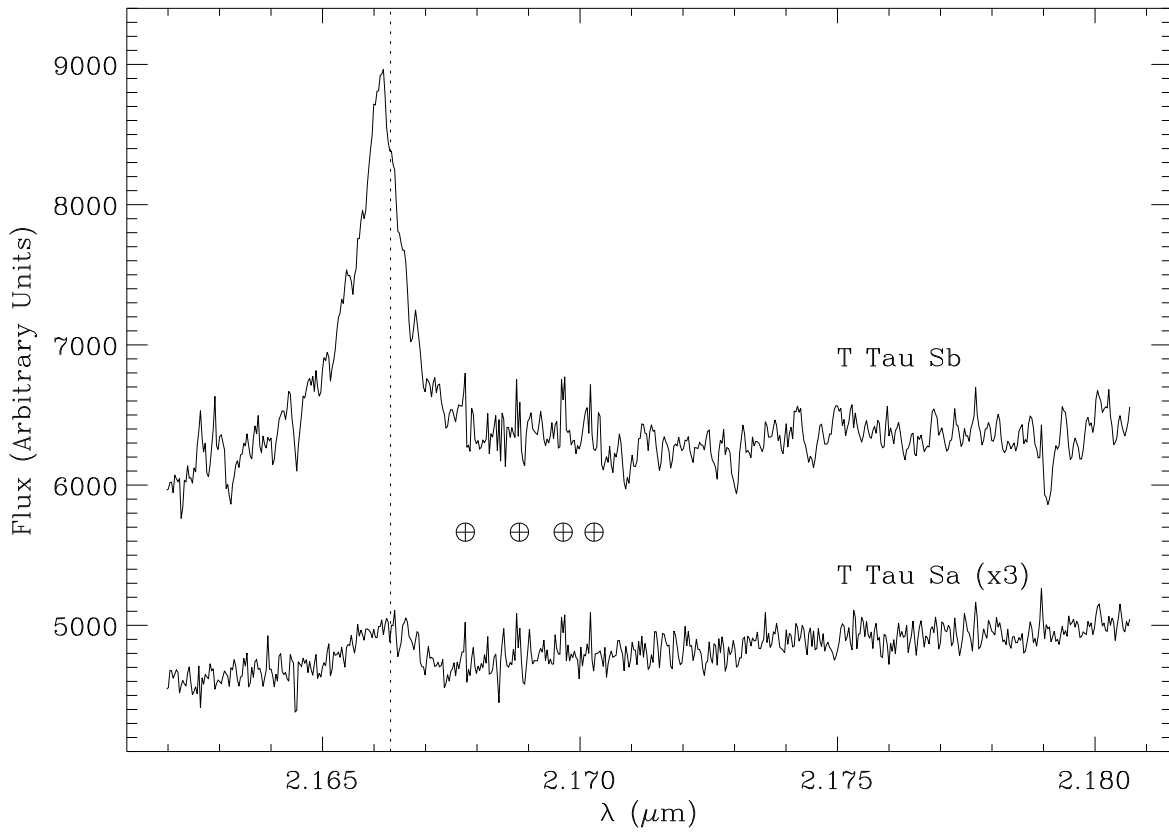


Fig. 6.— The spectra of T Tau Sa and T Tau Sb around the $\text{Br}\gamma$ emission line. The vertical dotted line indicates the rest velocity of T Tau Sb. A few spikes at wavelengths between 2.167 and 2.170 μm (labelled with a \oplus symbol) are due to an imperfect telluric absorption correction and are not intrinsic to the stars.

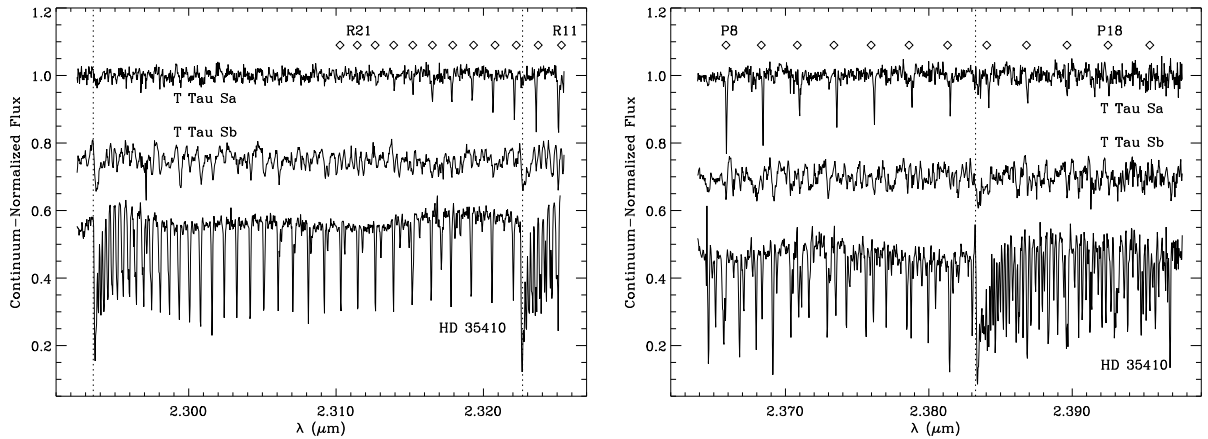


Fig. 7.— The spectra of T Tau Sa, T Tau Sb, and HD 35410, from top to bottom, in orders #4 (left) and #5 (right). They all have been continuum-normalized and shifted vertically by different amounts in the two orders for clarity. Vertical dotted lines indicate the location of the ^{12}CO bandheads while diamonds indicate $v = 2-0$ ^{12}CO individual transitions; the identification of the shortest and longest wavelength lines detected in each order of the spectrum of T Tau Sa is indicated.

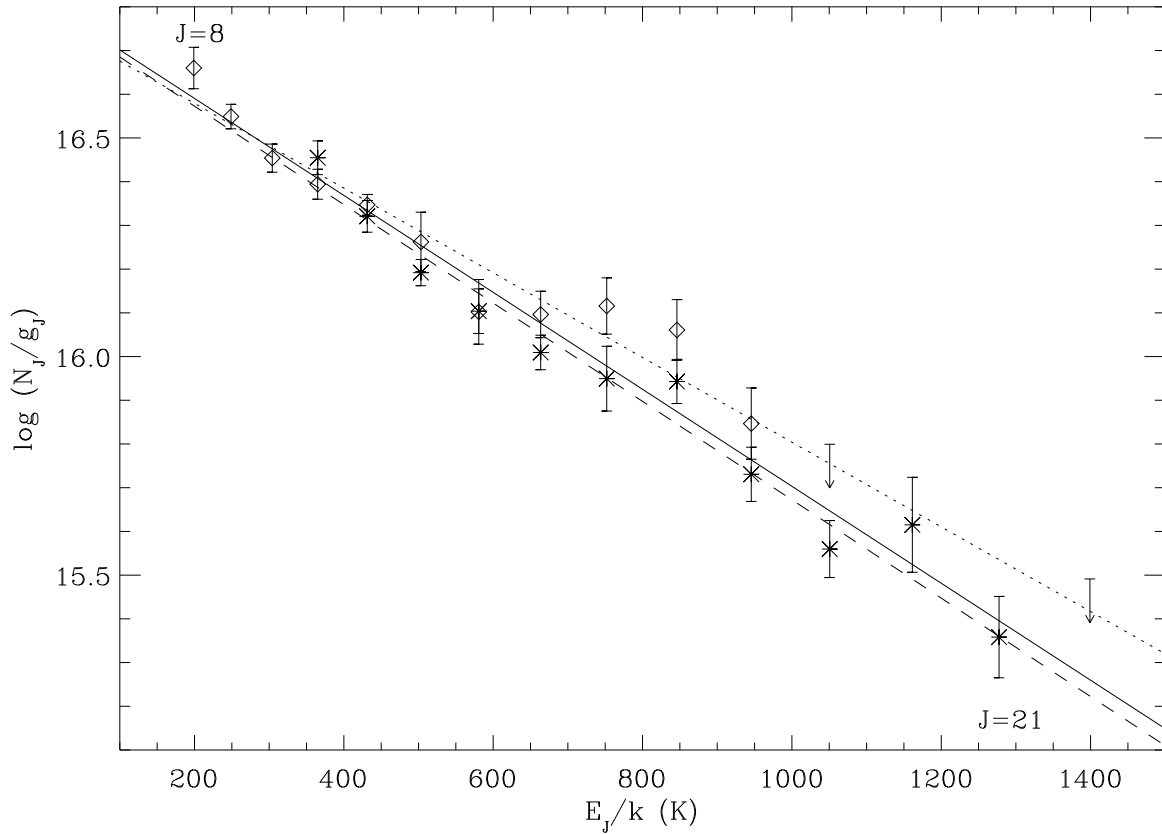


Fig. 8.— Rotational diagram for the ^{12}CO P - (diamonds) and R -lines (stars) in the spectrum of T Tau Sa. The dotted and dashed lines are linear fit to the P - and R -lines, respectively while the solid line (which corresponds to a gas temperature of 390 K and a total column density $N_{\text{CO}} = 9.0 \times 10^{18} \text{ cm}^{-2}$) is a simultaneous fit to all detected lines.

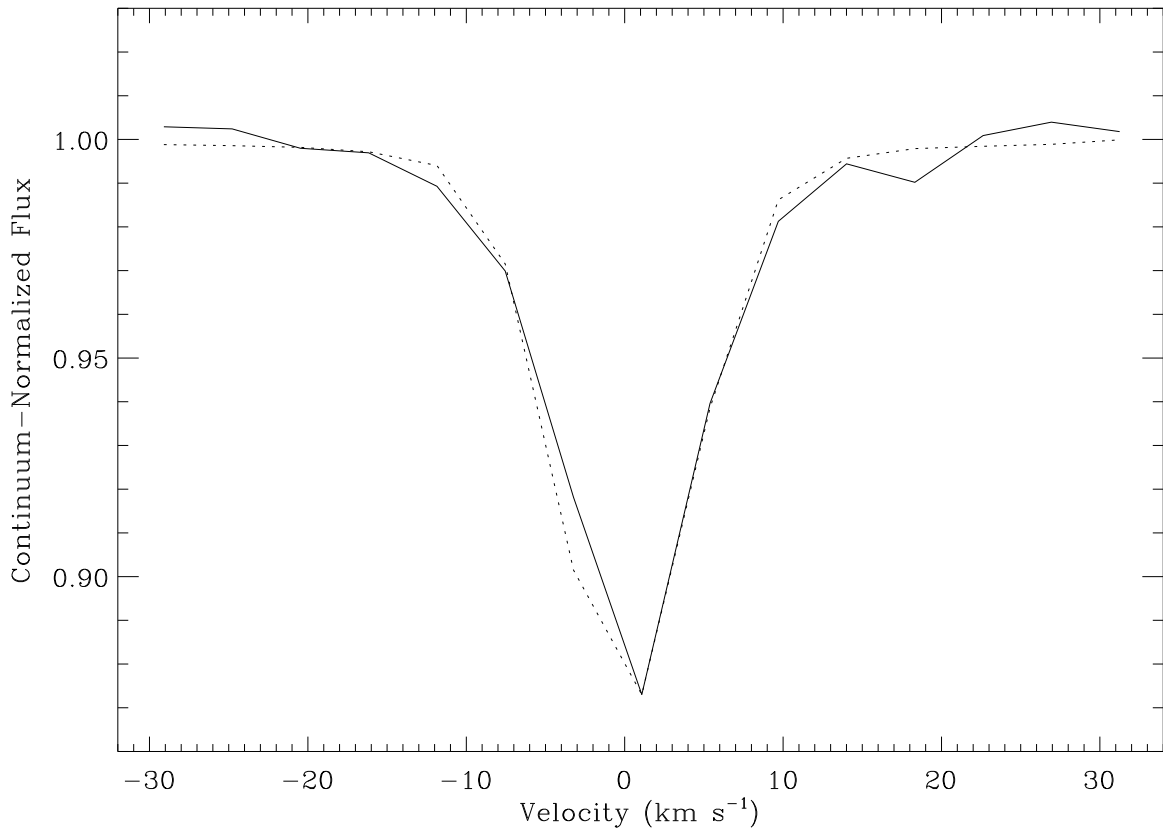


Fig. 9.— The EW-weighted average of the CO absorption line profiles (solid line) compared to that of the unresolved arc lamp lines (dotted line). Both profiles are averaged over all the features found in orders #4 and 5. The CO lines appear unresolved at our spectral resolution of $\sim 8.5 \text{ km s}^{-1}$.

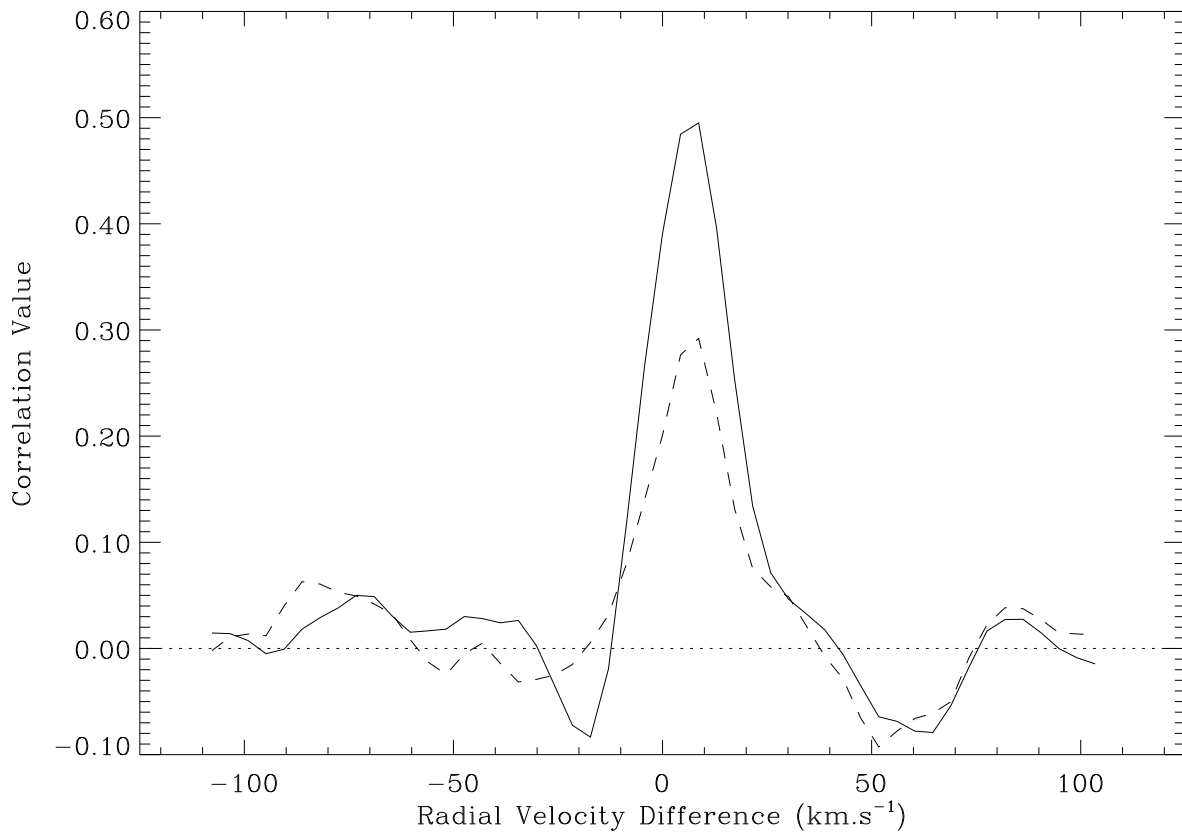


Fig. 10.— Cross-correlation functions for T Tau Sa (dashed curve) and T Tau Sb (solid curve) using HD 35410 as a template. The spectra from orders #4 and #5 were used simultaneously to obtain the cross-correlation functions. Both peaks are highly significant and no other peak of similar amplitude is detected even at high velocity shifts for either object.